

## RESEARCH ARTICLE OPEN ACCESS

# FLOWERS AEP: An Analytical Model for Wind Farm Layout Optimization

Michael J. LoCascio<sup>1</sup>  | Christopher J. Bay<sup>2</sup> | Luis A. Martínez-Tossas<sup>2</sup>  | Majid Bastankhah<sup>3</sup>  | Catherine Gorlé<sup>1</sup>

<sup>1</sup>Civil and Environmental Engineering, Stanford University, Stanford, California, USA | <sup>2</sup>National Wind Technology Center, National Renewable Energy Laboratory, Golden, Colorado, USA | <sup>3</sup>Department of Engineering, Durham University, Durham, UK

**Correspondence:** Michael J. LoCascio ([locascio@stanford.edu](mailto:locascio@stanford.edu))

**Received:** 6 May 2024 | **Revised:** 8 July 2024 | **Accepted:** 1 September 2024

**Funding:** This research was supported by the U.S. Department of Energy Office of Energy Efficiency and Renewable Energy Wind Energy Technologies Office.

**Keywords:** annual energy production | wake modeling | wind farm layout optimization

## ABSTRACT

Annual energy production (AEP) is commonly used in objective functions for wind farm layout optimization. AEP is proportional to wind farm power production integrated over an annual distribution of free-stream wind conditions. Physics-based estimates of wind farm power production typically rely on low-fidelity engineering wake models that approximate the steady-state wind farm flow field. AEP estimates are then obtained by performing independent simulations for discrete wind conditions and using rectangular quadrature to account for each condition's expected frequency of occurrence. Depending on the number of simulated discrete wind conditions, this numerical integral could be hampered by poor accuracy or high computational costs. The FLOWERS AEP model instead poses an analytical integral of the engineering wake model over the variable wind conditions, yielding a closed-form, analytical function for wind farm AEP. This paper derives the analytical functions for FLOWERS AEP and its derivatives with respect to turbine position, which are useful for gradient-based wind farm layout optimization, in nondimensional form. We then analyze the benefits of the FLOWERS AEP model over conventional reference models, focusing on its low cost, adequate wake loss predictions, and smooth design space. Although the FLOWERS approach is found to predict the exact value of AEP with some error relative to the reference model (within 14% on average), it dramatically reduces computation time by an order of magnitude, produces a qualitatively similar design space at relatively low resolution, and yields comparable optimal layouts. This significant speed improvement is critical in layout optimization applications, where determining an optimal layout in an efficient manner is more important than precise AEP prediction.

## 1 | Introduction

An important application of annual energy production (AEP) models is in wind farm layout optimization (WFLO) problems. In these studies, AEP can be an objective function to be maximized by optimizing over the placement of each turbine in the farm within a given boundary [1–3]. The energy production of a wind farm over a given period is a function of the ambient wind

conditions such as mean wind direction, mean wind speed, turbulence intensity, and atmospheric stability [4, 5]. These properties are highly variable and nonstationary over time scales of an hour or longer [6]. Therefore, a key challenge in estimating the expected energy production of a wind farm over longer time horizons (e.g., an operational lifetime of years) is in the accounting of these variable atmospheric conditions. In this framing, AEP—which refers to the energy content of the expected power

This is an open access article under the terms of the [Creative Commons Attribution](https://creativecommons.org/licenses/by/4.0/) License, which permits use, distribution and reproduction in any medium, provided the original work is properly cited.

© 2024 National Renewable Energy Laboratory and The Author(s). *Wind Energy* published by John Wiley & Sons Ltd.

production over the course of 1 year—is an uncertainty quantification problem for wind plant performance.

The power production of a wind plant is diminished by wake interactions between turbines. Wind turbines produce a turbulent wake, which imparts a deficit in the mean wind speed caused by the thrust of the rotor [7]. This wake velocity deficit—which dissipates with downstream distance as the wake mixes with the free-stream flow—characterizes a region of reduced kinetic energy density [5]. For a second turbine operating within this wake, the potential power production is reduced compared to operating in the free-stream flow. Power losses of 10%–20% [8] and up to 40% in the worst-case (i.e., aligned) wind directions [9, 10] have been documented in utility-scale wind farms.

Physics-based predictions of wind farm power production therefore require the modeling of the ambient wind conditions and the modeling of intrafarm wake interactions under these conditions. Low-fidelity engineering wake models are analytical functions derived from basic governing flow equations (such as conservation of mass and momentum) whose output is often dependent on parameterized wind turbine forcings and ambient turbulence [11–13] (see the review by Porté-Agel et al. [4] for detailed discussion on this topic). Because engineering wake models approximate the infinite time-averaged wind farm flow, the flow scenarios are limited to statistically stationary atmospheric conditions. To extend these modeling tools to an AEP estimate, the variability of these wind conditions must be accounted for. If the atmospheric conditions are defined by a set of uncertain variables  $\Gamma_{\infty}$ , and assuming the probability density function of the atmospheric conditions,  $f(\Gamma_{\infty})$ , is known, then AEP is proportional to the expectation (denoted by  $\mathbb{E}$ ) of power production of the wind farm  $P$  under the uncertainty of the steady-state conditions:

$$AEP \propto \mathbb{E}_{f(\Gamma_{\infty})}[P(\Gamma_{\infty})]. \quad (1)$$

The standard approach to evaluate the expectation of wind farm power production for AEP predictions relies on numerical integration. First, the probability density function of the wind conditions (viz., free-stream wind direction and wind speed) is estimated by discretizing historical data at the site of interest into a tabulated wind rose. Second, independent simulations are performed for each unique discrete atmospheric state. Finally, a weighted average of turbine power production is taken across all simulations according to the expected frequency of occurrence of each state, which is analogous to a midpoint rule numerical integration (i.e., rectangular quadrature) [14]. We refer to these AEP predictions based on the numerical integration of an underlying wind farm model as “Conventional” AEP models. This implementation is widely used for estimating AEP with high-fidelity simulations [15] or low-fidelity wake models [14, 16, 17] and is the internal method in state-of-the-art wake modeling libraries such as FLORIS [18] or PyWake [19].

An alternative approach first proposed in LoCascio et al. [20] introduced the FLOWERS model for annually averaged wind speed. The FLOWERS approach evaluates expected power production (Equation 1) with an analytical integral across wind

conditions instead of a numerical integral. The resulting analytical, closed-form expression for AEP reduces computational cost compared to the Conventional AEP modeling approach, and FLOWERS was found to predict AEP about an order of magnitude faster. One compelling application of the FLOWERS model is in the WFLO problem, where FLOWERS was found to reduce the computational costs of WFLO studies by an order of magnitude.

Our objective in this paper is to further advance and demonstrate the advantages of the reduced-order, design-oriented FLOWERS AEP model over Conventional AEP models for layout optimization. To achieve this objective, we first derive analytic functions for the gradient of the FLOWERS AEP model with respect to turbine position, which are ideal for gradient-based WFLO problems where the design variables are the position coordinates of individual turbines. In the process, we also update the derivation of FLOWERS AEP from the previous work [20] and express it in a nondimensional form. Next, we analyze how FLOWERS achieves three desirable characteristics of an AEP model in WFLO studies: (1) low cost, (2) adequate wake loss predictions, and (3) smooth design space. Lastly, we compare the performance of FLOWERS to Conventional AEP models in a simple layout optimization problem to demonstrate the potential advantage of the combination of cost savings, adequate accuracy, and smoothness. We expand on each of these characteristics in the remainder of this section.

First, the computational cost of a layout optimization study is nontrivial: The overall time required for these studies can easily exceed 24 h [21] and necessitate the use of high-performance computing. A straightforward way to reduce the cost of these studies is to reduce the cost of the objective function evaluation. This cost is determined by two factors: the cost of the model used to estimate power predictions under quasi-stationary conditions and the cost of the integration over the expected wind conditions. Considering the cost of the power prediction model, high-fidelity computational fluid dynamics simulations are prohibitively expensive for WFLO applications [22, 23]. Consequently, low-fidelity engineering wake models are the standard tool for these studies [15, 24–32], with evaluation times on the order of 1 second or less.

As for the integration, one limitation of the numerical integration approach of Conventional AEP models is that cost scales with the number of simulated discrete wind conditions. Some recent studies have focused on statistical methods to better sample discrete wind conditions for the numerical integral. Murcia et al. [14] and Padrón et al. [28] used polynomial chaos expansion to estimate AEP with significantly fewer simulations, while King et al. [33] used Bayesian quadrature for a similar purpose; these techniques were able to reduce the cost of the AEP estimate by 80%–95%. Another method by Quick et al. [29] used Monte Carlo integration in place of the basic rectangular quadrature to avoid the cost issues associated with the discretization of wind conditions. These methods are promising but are still limited to the fundamental numerical integral approach. We will use evaluations of random wind farm layout configurations across a variety of wind roses to quantify the cost savings that can be obtained through analytical evaluation of the integral enabled by FLOWERS.

Second, an AEP model must adequately capture the “wake avoidance” of a wind farm layout. As discussed in LoCascio et al. [20], the layout optimization problem can be conceptualized as a wake avoidance problem: The goal of the optimization study is to place turbines where they avoid the wakes of other turbines as much as possible. In this definition, the objective function is a reduced-order quantitative metric of wake avoidance that must be able to consistently map marginal changes in turbine position to marginal changes in wake losses. Therefore, the absolute accuracy of the AEP estimate is not essential, especially if the objective function is normalized by its initial value. We will use the analysis of the AEP predictions for the randomized wind farm layouts across the range of wind roses to determine FLOWERS’ capability to consistently identify the layouts that maximize AEP.

Third, an AEP model should be smooth with respect to turbine position. The WFLO problem is nonlinear, which produces a highly multimodal design space with numerous local solutions [31, 34]. Many WFLO studies leverage gradient-based algorithms that use gradients of the objective function to locate local optima [15, 21, 25–27, 31, 34, 35]. Numerical error in the integral within the objective function (Equation 1) or errors in gradient estimates can contribute spurious local optima or other undesirable features to the design space that make it more difficult for the optimizer to effectively locate local optima and satisfy optimality conditions.

Ideally, analytical functions of the gradients are available for gradient-based optimization. Guirguis et al. [36] derived the analytical gradients of a simplified Conventional AEP model for use in a WFLO study. If analytical functions are not available, gradients can be computed through automatic differentiation or complex step methods [37]; these gradient calculations are highly accurate but require the wake modeling code to be constructed in a way that is complementary to specialized automatic differentiation packages. Thomas et al. [38] addressed this point by modifying the wake model underlying their objective function to make it more suitable for automatic differentiation. The most straightforward option for gradient information is to estimate them with first- or second-order finite differences [37]. However, finite-difference gradients require one or two evaluations of the underlying function per dimension and possess nontrivial numerical error. We will compare the behavior of FLOWERS and Conventional AEP models across the design space for WFLO problems to determine their suitability as objective functions in WFLO problems.

The paper is organized as follows. Section 2 describes the derivation of the FLOWERS AEP model and its gradient with respect to turbine positions and the Conventional AEP models and differences in their modeling assumptions. Section 3 compares the FLOWERS and Conventional AEP models across the randomly generated cases with a focus on two quantities of interest: the AEP predictions themselves and the time required to evaluate the models. Section 4 demonstrates the behavior of these models as layout optimization objective functions and analyzes the design spaces they produce. Section 5 illustrates the performance of these models in a layout optimization case study. Finally, Section 6 outlines the key takeaways and conclusions.

## 2 | AEP Models

### 2.1 | FLOWERS AEP

#### 2.1.1 | AEP Function Derivation

We wish to generalize the definition of AEP in dimensionless form, which requires the identification of key scaling parameters. The relevant length scale is the rotor diameter of the turbines,  $D$ , because wake structures and their evolution with downstream distance are proportional to the rotor size. Our choice of velocity scale is the cut-out wind speed of the turbine,  $u_c$ , because the turbine control system sets an upper bound on the incident wind speed that yields nonzero power production. The air density,  $\rho$ , is assumed to be constant. Lastly, a unit conversion,  $Q$ , is necessary to relate expected power production to the proportional AEP ( $Q = 8760$  h per year to convert from W to Wh).

Based on these relevant scales, we identify key dimensionless parameters that fall into three categories: flow parameters, turbine parameters, and plant parameters. Regarding the flow, for a dimensional wind speed  $u$  and wind direction  $\phi$  (assuming units of radians), we obtain normalized wind speed  $\tilde{u}$  and direction  $\tilde{\phi}$  as follows:  $\tilde{u} = u/u_c$ ,  $\tilde{\phi} = \phi/2\pi$ . The effects of atmospheric boundary layer and wake-added turbulence on the wake behavior are parameterized with a tunable wake expansion rate,  $k$ . Also, we consider the joint probability density function of the uncertain free-stream wind direction and speed,  $f(\tilde{u}_\infty, \tilde{\phi}_\infty)$ , as previously defined. The turbine is modeled as an actuator disk and parameterized with thrust and power coefficients,  $C_T(\tilde{u})$  and  $C_P(\tilde{u})$ , respectively, which are functions of the incident normalized wind speed. Lastly, at the plant level, the positions of all turbines are defined by  $(\mathbf{x}, \mathbf{y})$ , where  $x$  and  $y$  are the easting and northing coordinates, respectively, and  $(x_i, y_i) \forall i \in \{1, \dots, N\}$  for  $N$  turbines in the plant. The coordinates are normalized by the rotor diameter as follows:  $\tilde{\mathbf{x}} = \mathbf{x}/D$ ,  $\tilde{\mathbf{y}} = \mathbf{y}/D$ .

We posit that the AEP of a wind farm can be expressed as a dimensionless function  $F$  of these dimensionless quantities:

$$\frac{AEP}{\frac{\pi}{8} Q \rho D^2 u_c^3} = F(\tilde{\mathbf{x}}, \tilde{\mathbf{y}}, C_P, C_T, k, f). \quad (2)$$

We make some initial assumptions to guide the derivation. First, the free-stream wind conditions,  $u_\infty$  and  $\phi_\infty$ , and the probability distribution,  $f(\tilde{u}_\infty, \tilde{\phi}_\infty)$ , are uniform across the wind plant. Second, the wake expansion parameter,  $k$ , is also uniform throughout the wind farm and does not depend on local turbulence intensity. Third, all turbines are assumed to be identical, with the same thrust and power curves, rotor diameter, and hub height. Lastly, we treat the rotor as a single point and consequently neglect the effects of wind shear, wind veer, and partial wake overlap.

A simple definition for the time-averaged power production of a wind turbine is a function of the incident wind speed (averaged across the rotor-swept area) cubed:

$$P_i = \frac{1}{2} C_P(u_i) \rho A u_i^3, \quad (3)$$

where  $P_i$  is the power production of turbine  $i$ ,  $u_i$  is the incident wind speed, and  $A$  is the rotor-swept area,  $A = \pi D^2/4$ . The local wind speed for a given turbine is the difference between the free-stream wind speed  $u_\infty$  and the total wake velocity deficit  $\Delta u_i$  caused by other turbines:  $u_i = u_\infty - \Delta u_i$ . In wind plants with many turbines interacting with each other, this total wake velocity deficit is the combined effect of several individual wake velocity deficits  $\Delta u_{ij}$  produced by turbines  $j$  in the neighbor set of  $i$ ,  $j \in \mathcal{N}_i$ . A wake velocity deficit only exists downwind of turbine  $j$ , so in general, the neighbor set  $\mathcal{N}_i$  contains all turbines upwind of turbine  $i$ :  $j \in \mathcal{N}_i$  if  $x_i - x_j > 0$ . Here, for simplicity and without the loss of generality, we assume that the wind is westerly, so the position coordinate  $x$  is aligned with the streamwise direction.

The relative orientation of turbines, which is determined by the free-stream wind direction  $\phi_\infty$ , defines the neighbor set underlying these wake interactions. Also, turbine power production and the magnitude of the wake deficits are a function of the free-stream wind speed  $u_\infty$ . Thus,  $\Delta u_i = \Delta u_i(u_\infty, \phi_\infty)$ , and the total power production of the wind farm is a function of these two atmospheric state variables:

$$P(u_\infty, \phi_\infty) = \sum_{i=1}^N P_i(u_\infty, \phi_\infty) = \frac{\pi}{8} \rho D^2 \sum_{i=1}^N C_P(u_i) [u_\infty - \Delta u_i(u_\infty, \phi_\infty)]^3. \quad (4)$$

Expected power production  $\bar{P}$  is the expected value of Equation (4) with respect to the probability density function  $f(u_\infty, \phi_\infty)$ . AEP is the total energy production over the course of 1 year at a rate  $\bar{P}$ , with the unit conversion  $Q$  to relate these two quantities:

$$AEP = \frac{\pi}{8} Q \rho D^2 \mathbb{E}_{f(u_\infty, \phi_\infty)} \left[ \sum_{i=1}^N C_P(u_i) [u_\infty - \Delta u_i(u_\infty, \phi_\infty)]^3 \right]. \quad (5)$$

The FLOWERS AEP model is based on the Jensen wake model [12], which defines the wake velocity deficit with a top-hat profile as follows:

$$\frac{\Delta u_{ij}}{u_\infty}(x_{ij}, y_{ij}) = \frac{1 - \sqrt{1 - C_T(u_j)}}{(2kx_{ij}/D + 1)^2} W(x_{ij}, y_{ij}). \quad (6)$$

The wind direction in this case is aligned with the positive  $x$  direction, so  $x$  and  $y$  are the streamwise and spanwise Cartesian coordinates, respectively.  $x_{ij}$  and  $y_{ij}$  are the relative position between turbines  $i$  and  $j$ :  $x_{ij} = x_i - x_j$ ,  $y_{ij} = y_i - y_j$ . The thrust coefficient  $C_T$  is a function of the wind speed incident on turbine  $j$  that produces the wake.  $W(x_{ij}, y_{ij})$  is a step function that represents the discrete wake region:

$$W = \begin{cases} 1, & x_{ij} \geq 0 \text{ and } |y_{ij}| \leq kx_{ij} + D/2, \\ 0, & \text{else.} \end{cases} \quad (7)$$

We convert Equation (6) into polar coordinates,  $r_{ij} = \sqrt{x_{ij}^2 + y_{ij}^2}$  and  $\theta_{ij} = \arctan\left(\frac{y_{ij}}{x_{ij}}\right)$ . We also relax the wake geometry definition to permit a variable wind direction  $\phi_\infty$ :

$$\frac{\Delta u_{ij}}{u_\infty}(r_{ij}, \theta_{ij}, \phi_\infty) = \frac{1 - \sqrt{1 - C_T(u_j)}}{(2kr_{ij} \cos(\theta_{ij} - \phi_\infty)/D + 1)^2} W(r_{ij}, \theta_{ij}, \phi_\infty). \quad (8)$$

We normalize the polar coordinates with the relevant scales,  $\tilde{r}_{ij} = r_{ij}/D$  and  $\tilde{\theta}_{ij} = \theta_{ij}/2\pi$ , to express Equation (8) in our dimensionless groups:

$$\frac{\Delta u_{ij}}{u_\infty}(\tilde{r}_{ij}, \tilde{\theta}_{ij}, \tilde{\phi}_\infty) = \frac{1 - \sqrt{1 - C_T(\tilde{u}_j)}}{(2k\tilde{r}_{ij} \cos[2\pi(\tilde{\theta}_{ij} - \tilde{\phi}_\infty)] + 1)^2} W(\tilde{r}_{ij}, \tilde{\theta}_{ij}, \tilde{\phi}_\infty). \quad (9)$$

The wake boundary in Equation (7) can be expressed in terms of a critical angle  $\tilde{\theta}_{ij}^{(c)}$  (which we define to be positive):

$$\tilde{r}_{ij} \sin(2\pi\tilde{\theta}_{ij}^{(c)}) = k\tilde{r}_{ij} \cos(2\pi\tilde{\theta}_{ij}^{(c)}) + \frac{1}{2}. \quad (10)$$

Solving for  $\tilde{\theta}_{ij}^{(c)}$ ,

$$\tilde{\theta}_{ij}^{(c)}(\tilde{r}_{ij}, k) = \frac{1}{2\pi} \arctan \left( \frac{\frac{1}{2\tilde{r}_{ij}} + k\sqrt{1 + k^2 - \left(\frac{1}{2\tilde{r}_{ij}}\right)^2}}{-\frac{k}{2\tilde{r}_{ij}} + \sqrt{1 + k^2 - \left(\frac{1}{2\tilde{r}_{ij}}\right)^2}} \right), \quad (11)$$

we recognize that  $W(\tilde{r}_{ij}, \tilde{\theta}_{ij}, \tilde{\phi}_\infty) = 1$  if  $|\tilde{\theta}_{ij} - \tilde{\phi}_\infty| \leq \tilde{\theta}_{ij}^{(c)}$  and is zero otherwise.

We use a linear combination of wake velocity deficits [39],

$$\Delta u_i = \sum_{j \in \mathcal{N}_i} \Delta u_{ij}. \quad (12)$$

Substituting Equations (9) and (12) into Equation (5),

$$AEP = \frac{\pi}{8} Q \rho D^2 34 \mathbb{E}_{f(\tilde{u}_\infty, \tilde{\phi}_\infty)} \left[ \sum_{i=1}^N C_P(\tilde{u}_i) \tilde{u}_\infty^3 \left[ 1 - \sum_{j=1, j \neq i}^N \frac{1 - \sqrt{1 - C_T(\tilde{u}_j)}}{(2k\tilde{r}_{ij} \cos[2\pi(\tilde{\theta}_{ij} - \tilde{\phi}_\infty)] + 1)^2} W(\tilde{r}_{ij}, \tilde{\theta}_{ij}, \tilde{\phi}_\infty) \right]^3 \right]. \quad (13)$$

Note that the wake region  $W$  now handles the definition of the neighbor set  $\mathcal{N}_i$  and so the summation over  $j$  has been relaxed to include all indices  $j \in \{1, 2, \dots, N\}$  (except  $i$ , because a turbine's wake cannot interact with itself).

Here, treating the thrust and power coefficients as a function of local wind speed,  $\tilde{u}_p$ , creates a coupled system of wake interactions; the incident wind speeds would need to be solved in a serial fashion before power is computed because the wake deficits are not independent of one another. To make these deficits independent, we approximate  $C_P(\tilde{u}_i) \approx C_P(\tilde{u}_\infty)$  and  $C_T(\tilde{u}_i) \approx C_T(\tilde{u}_\infty)$ . We note that this approximation is consistent with operation near Region II of the power curve, where aerodynamic efficiency is optimal.

To evaluate the expectation in Equation (13), we integrate over the probability distribution  $f(\tilde{u}_\infty, \tilde{\phi}_\infty)$ :

$$AEP = \frac{\pi}{8} Q \rho D^2 \tilde{u}_c^3 \sum_{i=1}^N \int \int_{\tilde{u}_\infty, \tilde{\phi}_\infty} C_P(\tilde{u}_\infty) \tilde{u}_\infty^3 \left[ 1 - \sum_{j=1, j \neq i}^N \frac{1 - \sqrt{1 - C_T(\tilde{u}_\infty)}}{(2k\tilde{r}_{ij} \cos[2\pi(\tilde{\theta}_{ij} - \tilde{\phi}_\infty)] + 1)^2} W(\tilde{r}_{ij}, \tilde{\theta}_{ij}, \tilde{\phi}_\infty) \right]^3 f(\tilde{u}_\infty, \tilde{\phi}_\infty) d\tilde{u}_\infty d\tilde{\phi}_\infty. \quad (14)$$

The integral over this cubic expansion is intractable because the elements of the summation over  $j$  in the integrand are not independent. We simplify by switching the order of the integration and the cubic expansion, resulting in the following expression:

$$AEP = \frac{\pi}{8} Q \rho D^2 u_c^3 \sum_{i=1}^N \left[ \int_{\tilde{u}_\infty \tilde{\phi}_\infty} C_P^{1/3}(\tilde{u}_\infty) \tilde{u}_\infty f(\tilde{u}_\infty, \tilde{\phi}_\infty) d\tilde{u}_\infty d\tilde{\phi}_\infty - \sum_{j=1, j \neq i}^N \int_{\tilde{u}_\infty \tilde{\phi}_\infty} C_P^{1/3}(\tilde{u}_\infty) \tilde{u}_\infty \left[ \frac{1 - \sqrt{1 - C_T(\tilde{u}_\infty)}}{(2k\tilde{r}_{ij} \cos[2\pi(\tilde{\theta}_{ij} - \tilde{\phi}_\infty)] + 1)^2} W(\tilde{r}_{ij}, \tilde{\theta}_{ij}, \tilde{\phi}_\infty) \right] f(\tilde{u}_\infty, \tilde{\phi}_\infty) d\tilde{u}_\infty d\tilde{\phi}_\infty \right]^3 \quad (15)$$

After rearranging and defining two main terms, we arrive at the following expression that conforms to the functional form posed in Equation (2):

$$F = \frac{AEP}{\frac{\pi}{8} Q \rho D^2 u_c^3} = \sum_{i=1}^N \left[ \bar{p}_\infty - \sum_{j=1, j \neq i}^N \overline{\Delta p_{ij}}(\tilde{r}_{ij}, \tilde{\theta}_{ij}) \right]^3 \quad (16)$$

The first term  $\bar{p}_\infty$  represents the maximum possible AEP assuming zero wake losses. The second term  $\overline{\Delta p_{ij}}$  is the expected contribution of wake losses. The overbar  $\bar{*}$  indicates an expected quantity (i.e., mean) as a result of an integral over the domain of wind conditions.

The definition of  $\bar{p}_\infty$ ,

$$\bar{p}_\infty = \int \int_{\tilde{u}_\infty \tilde{\phi}_\infty} C_P^{1/3}(\tilde{u}_\infty) \tilde{u}_\infty f(\tilde{u}_\infty, \tilde{\phi}_\infty) d\tilde{u}_\infty d\tilde{\phi}_\infty, \quad (17)$$

represents the expected power production of a freestanding turbine and is primarily a function of the wind rose. The probability distribution is typically approximated by historical data at the site of interest (i.e., a wind rose). The free-stream wind speed and wind direction are discretized into uniformly spaced bins:  $u_\infty^{(s)} \forall s \in \{1, \dots, S\}$ ,  $\phi_\infty^{(d)} \forall d \in \{1, \dots, D\}$ . The frequency of occurrence of each discrete atmospheric state ( $u_\infty^{(s)}, \phi_\infty^{(d)}$ ) is tabulated over a sufficiently long measurement period to approximate the true probability distribution,  $f(u_\infty, \phi_\infty) \approx f(u_\infty^{(s)}, \phi_\infty^{(d)})$ . With this discretized probability density function, this double integral simply becomes a weighted sum across each discrete wind condition:

$$\bar{p}_\infty = \sum_{s=1}^S \sum_{d=1}^D f(\tilde{u}_\infty^{(s)}, \tilde{\phi}_\infty^{(d)}) C_P^{1/3}(\tilde{u}_\infty^{(s)}) \tilde{u}_\infty^{(s)}. \quad (18)$$

For the wake deficit term,

$$\overline{\Delta p_{ij}}(\tilde{r}_{ij}, \tilde{\theta}_{ij}) = \int \int_{\tilde{u}_\infty \tilde{\phi}_\infty} C_P^{1/3}(\tilde{u}_\infty) \tilde{u}_\infty \left[ \frac{1 - \sqrt{1 - C_T(\tilde{u}_\infty)}}{(2k\tilde{r}_{ij} \cos[2\pi(\tilde{\theta}_{ij} - \tilde{\phi}_\infty)] + 1)^2} W(\tilde{r}_{ij}, \tilde{\theta}_{ij}, \tilde{\phi}_\infty) \right] f(\tilde{u}_\infty, \tilde{\phi}_\infty) d\tilde{u}_\infty d\tilde{\phi}_\infty, \quad (19)$$

we make the simplification to use the average free-stream wind speed per wind direction,  $\hat{u}_\infty$ , to reduce the

integration to a single variable. The probability density function  $f(u_\infty, \phi_\infty)$  then becomes solely a function of wind direction,  $f(\phi_\infty)$ :

$$f(\phi_\infty^{(d)}) = \sum_{s=1}^S f(u_\infty^{(s)}, \phi_\infty^{(d)}), \quad (20)$$

$$\hat{u}_\infty(\phi_\infty^{(d)}) = \frac{1}{f(\phi_\infty^{(d)})} \sum_{s=1}^S \tilde{u}_\infty^{(s)} f(u_\infty^{(s)}, \phi_\infty^{(d)}). \quad (21)$$

This average free-stream wind speed is substituted into Equation (19):

$$\overline{\Delta p_{ij}}(\tilde{r}_{ij}, \tilde{\theta}_{ij}) = \int_{\tilde{\phi}_\infty} C_P^{1/3}(\hat{u}_\infty(\tilde{\phi}_\infty^{(d)})) \hat{u}_\infty(\tilde{\phi}_\infty^{(d)}) \left[ \frac{1 - \sqrt{1 - C_T(\hat{u}_\infty(\tilde{\phi}_\infty^{(d)}))}}{(2k\tilde{r}_{ij} \cos[2\pi(\tilde{\theta}_{ij} - \tilde{\phi}_\infty)] + 1)^2} W(\tilde{r}_{ij}, \tilde{\theta}_{ij}, \tilde{\phi}_\infty) \right] f(\tilde{\phi}_\infty^{(d)}) d\tilde{\phi}_\infty. \quad (22)$$

A portion of this term is solely a function of the discrete wind direction  $\tilde{\phi}_\infty^{(d)}$ . We introduce a discrete Fourier transform to express these discrete inputs in a continuous and analytical form:

$$c(\tilde{\phi}_\infty) \equiv C_P^{1/3}(\hat{u}_\infty(\tilde{\phi}_\infty^{(d)})) \hat{u}_\infty(\tilde{\phi}_\infty^{(d)}) \left[ 1 - \sqrt{1 - C_T(\hat{u}_\infty(\tilde{\phi}_\infty^{(d)}))} \right] \quad (23)$$

$$f(\tilde{\phi}_\infty^{(d)}) = \frac{a_0}{2} + \sum_{m=1}^{M-1} a_m \cos(2\pi m \tilde{\phi}_\infty) + b_m \sin(2\pi m \tilde{\phi}_\infty),$$

where  $a_0$ ,  $a_m$ , and  $b_m$  are the Fourier coefficients and  $M$  is the number of Fourier modes. Note that  $c(\tilde{\phi}_\infty)$  is a continuous function of the wind direction while the wind rose is restricted to a discrete space. Substituting into Equation (22),

$$\overline{\Delta p_{ij}}(\tilde{r}_{ij}, \tilde{\theta}_{ij}) = \int_0^1 c(\tilde{\phi}_\infty) \left[ \frac{1}{(2k\tilde{r}_{ij} \cos[2\pi(\tilde{\theta}_{ij} - \tilde{\phi}_\infty)] + 1)^2} W(\tilde{r}_{ij}, \tilde{\theta}_{ij}, \tilde{\phi}_\infty) \right] d\tilde{\phi}_\infty. \quad (24)$$

We introduce a change of the integration variable  $\alpha \equiv \tilde{\theta}_{ij} - \tilde{\phi}_\infty$ , which represents the normalized polar angle relative to the wind direction. Recall that the wake velocity deficit is zero for  $|\alpha| > \tilde{\theta}_{ij}^{(c)}$ , so we can replace the integration bounds with  $\pm \tilde{\theta}_{ij}^{(c)}$  and remove the step function  $W$ :

$$\overline{\Delta p_{ij}}(\tilde{r}_{ij}, \tilde{\theta}_{ij}) = \int_{-\tilde{\theta}_{ij}^{(c)}}^{\tilde{\theta}_{ij}^{(c)}} c(\tilde{\theta}_{ij} - \alpha) \left[ \frac{1}{(2k\tilde{r}_{ij} \cos(2\pi\alpha) + 1)^2} \right] d\alpha. \quad (25)$$

We approximate the fraction with a fourth-order Taylor series expansion to simplify the integration:

$$\frac{1}{(2k\tilde{r}_{ij}\cos(2\pi\alpha)+1)^2} = \frac{1}{(2k\tilde{r}_{ij}+1)^2} + 8\pi^2 \frac{k\tilde{r}_{ij}\alpha^2}{(2k\tilde{r}_{ij}+1)^3} + \mathcal{O}(\alpha^4). \quad (26)$$

Because the magnitude of  $\alpha$  is already limited by the bounds of  $\pm \tilde{\theta}_{ij}^{(c)}$  and is defined to be less than one, the error of this approximation is small.

At this point, the analytical integral looks as follows:

$$\begin{aligned} \overline{\Delta p}_{ij}(\tilde{r}_{ij}, \tilde{\theta}_{ij}) &= \int_{-\tilde{\theta}_{ij}^{(c)}}^{\tilde{\theta}_{ij}^{(c)}} \left[ \frac{a_0}{2} + \sum_{m=1}^{M-1} a_m \cos[2\pi m(\tilde{\theta}_{ij} - \alpha)] + b_m \sin[2\pi m(\tilde{\theta}_{ij} - \alpha)] \right] \\ &\quad \left[ \frac{1}{(2k\tilde{r}_{ij}+1)^2} + 8\pi^2 \frac{k\tilde{r}_{ij}\alpha^2}{(2k\tilde{r}_{ij}+1)^3} \right] d\alpha. \end{aligned} \quad (27)$$

We omit the details of the integration for brevity, yielding the following solution:

$$\begin{aligned} \overline{\Delta p}_{ij}(\tilde{r}_{ij}, \tilde{\theta}_{ij}) &= \frac{a_0 \tilde{\theta}_{ij}^{(c)}}{(2k\tilde{r}_{ij}+1)^2} \left[ 1 + \frac{8\pi^2 k\tilde{r}_{ij} \tilde{\theta}_{ij}^{(c)2}}{3(2k\tilde{r}_{ij}+1)} \right] \\ &\quad + \sum_{m=1}^{M-1} \left[ \frac{1}{\pi m(2k\tilde{r}_{ij}+1)^2} \{ a_m \cos(2\pi m\tilde{\theta}_{ij}) + b_m \sin(2\pi m\tilde{\theta}_{ij}) \} \left\{ \sin(2\pi m\tilde{\theta}_{ij}^{(c)}) \right. \right. \\ &\quad \left. \left. + \frac{2k\tilde{r}_{ij}}{m^2(2k\tilde{r}_{ij}+1)} \left[ (2\pi m\tilde{\theta}_{ij}^{(c)})^2 - 2 \right] \sin(2\pi m\tilde{\theta}_{ij}^{(c)}) + 4\pi m\tilde{\theta}_{ij}^{(c)} \cos(2\pi m\tilde{\theta}_{ij}^{(c)}) \right\} \right]. \end{aligned} \quad (28)$$

Together, Equations (16), (18), and (28) compose the closed-form analytical function for AEP.

### 2.1.2 | AEP Gradient Derivation

We are interested in the partial derivatives of AEP with respect to the two independent coordinates of each turbine:  $\partial AEP / \partial \mathbf{x}$  and  $\partial AEP / \partial \mathbf{y}$ . In terms of our dimensionless quantities,

$$\frac{\partial AEP}{\partial \mathbf{x}} = \frac{\partial F}{\partial \tilde{\mathbf{x}}} \frac{\partial AEP}{\partial F} \frac{\partial \tilde{\mathbf{x}}}{\partial \mathbf{x}} = \frac{\pi}{8} Q \rho D u_c^3 \frac{\partial F}{\partial \tilde{\mathbf{x}}}, \quad (29)$$

$$\frac{\partial AEP}{\partial \mathbf{y}} = \frac{\partial F}{\partial \tilde{\mathbf{y}}} \frac{\partial AEP}{\partial F} \frac{\partial \tilde{\mathbf{y}}}{\partial \mathbf{y}} = \frac{\pi}{8} Q \rho D u_c^3 \frac{\partial F}{\partial \tilde{\mathbf{y}}}. \quad (30)$$

Considering an individual turbine  $g \in \{1, 2, \dots, N\}$ , we use the chain rule to expand these partial derivatives in terms of  $\tilde{r}_{ij}$  and  $\tilde{\theta}_{ij}$ , the position coordinates with which we define  $F$  in Equation (16):

$$\frac{\partial F}{\partial \tilde{\mathbf{x}}_g} = -3 \sum_{i=1}^N \left[ \left[ \bar{p}_\infty - \sum_{j=1, j \neq i}^N \overline{\Delta p}_{ij}(\tilde{r}_{ij}, \tilde{\theta}_{ij}) \right]^2 \sum_{j=1, j \neq i}^N \left[ \frac{\partial \overline{\Delta p}_{ij}}{\partial \tilde{r}_{ij}} \frac{\partial \tilde{r}_{ij}}{\partial \tilde{\mathbf{x}}_g} + \frac{\partial \overline{\Delta p}_{ij}}{\partial \tilde{\theta}_{ij}} \frac{\partial \tilde{\theta}_{ij}}{\partial \tilde{\mathbf{x}}_g} \right] \frac{\partial \tilde{\mathbf{x}}_{ij}}{\partial \tilde{\mathbf{x}}_g} \right], \quad (31)$$

$$\frac{\partial F}{\partial \tilde{\mathbf{y}}_g} = -3 \sum_{i=1}^N \left[ \left[ \bar{p}_\infty - \sum_{j=1, j \neq i}^N \overline{\Delta p}_{ij}(\tilde{r}_{ij}, \tilde{\theta}_{ij}) \right]^2 \sum_{j=1, j \neq i}^N \left[ \frac{\partial \overline{\Delta p}_{ij}}{\partial \tilde{r}_{ij}} \frac{\partial \tilde{r}_{ij}}{\partial \tilde{\mathbf{y}}_g} + \frac{\partial \overline{\Delta p}_{ij}}{\partial \tilde{\theta}_{ij}} \frac{\partial \tilde{\theta}_{ij}}{\partial \tilde{\mathbf{y}}_g} \right] \frac{\partial \tilde{\mathbf{y}}_{ij}}{\partial \tilde{\mathbf{y}}_g} \right]. \quad (32)$$

The last partial derivative in these expressions accounts for the movement of the individual turbine  $g$ :

$$\frac{\partial \tilde{\mathbf{x}}_{ij}}{\partial \tilde{\mathbf{x}}_g} = \frac{\partial \tilde{\mathbf{y}}_{ij}}{\partial \tilde{\mathbf{y}}_g} = \begin{cases} 1, & g=i, \\ -1, & g=j, \\ 0, & \text{else.} \end{cases} \quad (33)$$

From the previous definitions of  $\tilde{r}_{ij}$  and  $\tilde{\theta}_{ij}$ , we obtain the following partial derivatives:

$$\frac{\partial \tilde{r}_{ij}}{\partial \tilde{\mathbf{x}}_{ij}} = \frac{\tilde{\mathbf{x}}_{ij}}{\tilde{r}_{ij}}, \quad (34)$$

$$\frac{\partial \tilde{r}_{ij}}{\partial \tilde{\mathbf{y}}_{ij}} = \frac{\tilde{\mathbf{y}}_{ij}}{\tilde{r}_{ij}}, \quad (35)$$

$$\frac{\partial \tilde{\theta}_{ij}}{\partial \tilde{\mathbf{x}}_{ij}} = -\frac{\tilde{\mathbf{y}}_{ij}}{2\pi \tilde{r}_{ij}^2}, \quad (36)$$

$$\frac{\partial \tilde{\theta}_{ij}}{\partial \tilde{\mathbf{y}}_{ij}} = \frac{\tilde{\mathbf{x}}_{ij}}{2\pi \tilde{r}_{ij}^2}. \quad (37)$$

Substituting these equations into Equations (31) and (32), we can write the derivatives as follows:

$$\frac{\partial F}{\partial \tilde{\mathbf{x}}_g} = -3 \sum_{i=1}^N \left[ \left[ \bar{p}_\infty - \sum_{j=1, j \neq i}^N \overline{\Delta p}_{ij}(\tilde{r}_{ij}, \tilde{\theta}_{ij}) \right]^2 \sum_{j=1, j \neq i}^N \left[ \frac{\partial \overline{\Delta p}_{ij}}{\partial \tilde{r}_{ij}} \frac{\tilde{\mathbf{x}}_{ij}}{\tilde{r}_{ij}} - \frac{\partial \overline{\Delta p}_{ij}}{\partial \tilde{\theta}_{ij}} \frac{\tilde{\mathbf{y}}_{ij}}{2\pi \tilde{r}_{ij}^2} \right] \frac{\partial \tilde{\mathbf{x}}_{ij}}{\partial \tilde{\mathbf{x}}_g} \right], \quad (38)$$

$$\frac{\partial F}{\partial \tilde{\mathbf{y}}_g} = -3 \sum_{i=1}^N \left[ \left[ \bar{p}_\infty - \sum_{j=1, j \neq i}^N \overline{\Delta p}_{ij}(\tilde{r}_{ij}, \tilde{\theta}_{ij}) \right]^2 \sum_{j=1, j \neq i}^N \left[ \frac{\partial \overline{\Delta p}_{ij}}{\partial \tilde{r}_{ij}} \frac{\tilde{\mathbf{y}}_{ij}}{\tilde{r}_{ij}} + \frac{\partial \overline{\Delta p}_{ij}}{\partial \tilde{\theta}_{ij}} \frac{\tilde{\mathbf{x}}_{ij}}{2\pi \tilde{r}_{ij}^2} \right] \frac{\partial \tilde{\mathbf{y}}_{ij}}{\partial \tilde{\mathbf{y}}_g} \right]. \quad (39)$$

We see from Equations (38) and (39) that the derivatives of  $F$  with respect to either coordinate are both in terms of partial derivatives of  $\overline{\Delta p_{ij}}$  with respect to the relative polar coordinates  $\tilde{r}_{ij}$  and  $\tilde{\theta}_{ij}$ . For the partial derivative with respect to  $\tilde{\theta}_{ij}$ ,

$$\frac{\partial \overline{\Delta p_{ij}}}{\partial \tilde{\theta}_{ij}} = \sum_{m=1}^{M-1} \left[ \frac{2}{(2k\tilde{r}_{ij}+1)^2} \{b_m \cos(2\pi m\tilde{\theta}_{ij}) - a_m \sin(2\pi m\tilde{\theta}_{ij})\} \left\{ \sin(2\pi m\tilde{\theta}_{ij}^{(c)}) \right. \right. \\ \left. \left. + \frac{2k\tilde{r}_{ij}}{m^2(2k\tilde{r}_{ij}+1)} \left[ \left( (2\pi m\tilde{\theta}_{ij}^{(c)})^2 - 2 \right) \sin(2\pi m\tilde{\theta}_{ij}^{(c)}) + 4\pi m\tilde{\theta}_{ij}^{(c)} \cos(2\pi m\tilde{\theta}_{ij}^{(c)}) \right] \right\} \right]. \quad (40)$$

For the partial derivative with respect to  $\tilde{r}_{ij}$ , recall from Equation (11) that  $\tilde{\theta}_{ij}^{(c)} = \tilde{\theta}_{ij}^{(c)}(\tilde{r}_{ij}, k)$ . So we also require the partial derivative of  $\tilde{\theta}_{ij}^{(c)}$  with respect to  $\tilde{r}_{ij}$ :

$$\frac{\partial \tilde{\theta}_{ij}^{(c)}}{\partial \tilde{r}_{ij}} = - \frac{1}{4\pi \tilde{r}_{ij}^2 \sqrt{k^2 - \left(\frac{1}{2\tilde{r}_{ij}}\right)^2 + 1}}. \quad (41)$$

This expression allows us to derive the partial derivative of  $\overline{\Delta p_{ij}}$ :

$$\frac{\partial \overline{\Delta p_{ij}}}{\partial \tilde{r}_{ij}} = \frac{a_0}{3(2k\tilde{r}_{ij}+1)^4} \left\{ -4k\tilde{\theta}_{ij}^{(c)} \left[ 3 + 6k\tilde{r}_{ij} + 2\pi^2 \tilde{\theta}_{ij}^{(c)2} (4k\tilde{r}_{ij} - 1) \right] + 3(2k\tilde{r}_{ij} + 1) \left[ 1 + 2k\tilde{r}_{ij} + 8\pi^2 k\tilde{r}_{ij} \tilde{\theta}_{ij}^{(c)2} \right] \frac{\partial \tilde{\theta}_{ij}^{(c)}}{\partial \tilde{r}_{ij}} \right\} \\ + \sum_{m=1}^{M-1} \left\{ \frac{1}{\pi m^3 (2k\tilde{r}_{ij} + 1)^4} \right\} \left\{ a_m \cos(2\pi m\tilde{\theta}_{ij}) + b_m \sin(2\pi m\tilde{\theta}_{ij}) \right\} \\ \left\{ -4k \sin(2\pi m\tilde{\theta}_{ij}^{(c)}) \left[ 1 + m^2 + 2k\tilde{r}_{ij}(m^2 - 2) + 2\pi^2 m^2 \tilde{\theta}_{ij}^{(c)2} (4k\tilde{r}_{ij} - 1) \right] \right. \\ \left. + 2\pi m \cos(2\pi m\tilde{\theta}_{ij}^{(c)}) \left[ 4k\tilde{\theta}_{ij}^{(c)}(1 - 4k\tilde{r}_{ij}) + m^2(2k\tilde{r}_{ij} + 1) \left( 1 + 2k\tilde{r}_{ij} + 8\pi^2 k\tilde{r}_{ij} \tilde{\theta}_{ij}^{(c)2} \right) \frac{\partial \tilde{\theta}_{ij}^{(c)}}{\partial \tilde{r}_{ij}} \right] \right\}. \quad (42)$$

All together, Equations (33) and (38)–(42) represent the gradient elements  $\partial F / \partial \tilde{x}_g$  and  $\partial F / \partial \tilde{y}_g \forall g = \{1, 2, \dots, N\}$ .

## 2.2 | Conventional AEP

The Conventional AEP models evaluate expected power production (Equation 5) with a numerical integral over discrete

wind conditions. In this paper, we assume that our Conventional models also use the linear combination of wake velocity deficits (Equation 12) to maintain some consistency across the models.

Mathematically, the Conventional AEP models are defined as follows:

$$AEP = \frac{\pi}{8} Q \rho D^2 \sum_{d=1}^D \sum_{s=1}^S \sum_{i=1}^N \\ \left[ C_p(u_i(u_\infty^{(s)}, \phi_\infty^{(d)})) u_\infty^{(s)3} \left[ 1 - \sum_{j \in \mathcal{N}_i(\phi_\infty^{(d)})} \frac{\Delta u_{ij}(u_\infty^{(s)}, \phi_\infty^{(d)})}{u_\infty^{(s)}} \right]^3 \right] f(u_\infty^{(s)}, \phi_\infty^{(d)}). \quad (43)$$

We make similar simplifications to the Conventional AEP model for use in WFLO, namely, the average free-stream wind speed per wind direction, single rotor point, and horizontally homogeneous wind conditions.

To support our objectives, we consider two choices for the underlying model of the wake velocity deficit, as seen in Figure 1. The first

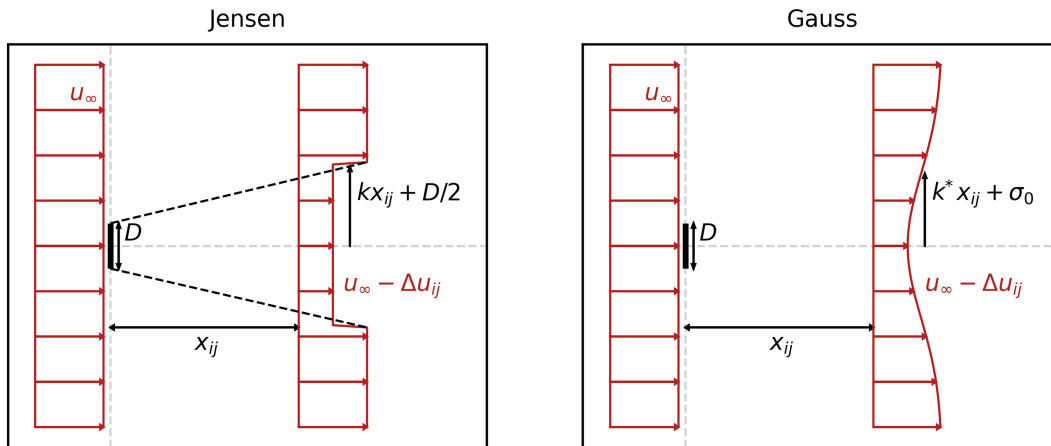


**FIGURE 1** | Two methods for a wake velocity deficit model to predict wind farm power production: the discrete, top-hat Jensen model (left) and the continuous Gauss model (right).

is the Jensen model (Equation 6), which is the same underlying wake model used by FLOWERS; the combination of Equations (6) and (43) will be referred to as the ‘‘Conventional-Jensen’’ model. The second is a Gaussian wake model [11], which has been found to better predict the flow distribution of the wake compared to the Jensen model. The Gaussian model defines the wake velocity deficit with a continuous, axisymmetric Gaussian profile:

$$\frac{\Delta u_{ij}(x_{ij}, y_{ij})}{u_{\infty}} = \left( 1 - \sqrt{1 - \frac{C_T(u_j)}{8(\sigma(x_{ij})/D)^2}} \right) \exp\left( -\frac{y_{ij}^2}{2\sigma(x_{ij})^2} \right), \quad (44)$$

where  $\sigma(x_{ij}) = k^*(x_{ij} - x_0) + D/\sqrt{8}$  is the spanwise wake width and  $x_0 = x_0(C_T(u_j))$  is the potential core length. The wake expansion parameter  $k^*$  is empirically modeled as a function of local incoming turbulence intensity  $I$  [40]:  $k^* = 0.38I + 0.004$ . Local turbulence intensity  $I$  is a combination of ambient turbulence intensity and wake-added turbulence intensity by upwind turbines, which is also modeled empirically [41]. Therefore, unlike the Jensen model, this form of the Gaussian model accounts for the development of wakes within the wind farm. We refer to the combination of Equations (43) and (44) as the ‘‘Conventional-Gauss’’ model.

## 2.3 | Modeling Discussion

As discussed previously, low-fidelity wake models are derived from a series of assumptions on the governing flow equations and turbine properties. In this section, we first outline the assumptions specific to the FLOWERS model to support the subsequent comparison with the Conventional AEP models. Second, we discuss some shared assumptions concerning the inputs to both of these AEP models.

### 2.3.1 | FLOWERS Assumptions

There are a few key assumptions in the derivation of the FLOWERS AEP model that contribute modeling error compared to the Conventional AEP models. The most significant approximation comes between Equations (14) and (15), when the order of the integration over wind directions and the nonlinear relationship with wind speed are swapped. In simplified terms, FLOWERS makes the approximation to substitute  $\left[ \frac{\hat{u}_{\infty}(1 - \Delta u_i / \hat{u}_{\infty})}{\hat{u}_{\infty}} \right]^3$  for  $\left[ \frac{\hat{u}_{\infty}(1 - \Delta u_i / \hat{u}_{\infty})}{\hat{u}_{\infty}} \right]^3$ . When  $f(\phi_{\infty})$  and  $\hat{u}_{\infty}(\phi_{\infty})$  vary across wind directions (which is the dimension over which we average), the Conventional approach is in fact the mathematical upper bound on the FLOWERS approach:  $\left[ \frac{\hat{u}_{\infty}(1 - \Delta u_i / \hat{u}_{\infty})}{\hat{u}_{\infty}} \right]^3 \leq \left[ \frac{\hat{u}_{\infty}(1 - \Delta u_i / \hat{u}_{\infty})}{\hat{u}_{\infty}} \right]^3$ ; less uniform distributions of  $f(\phi_{\infty})$  (i.e., wind roses with dominant wind directions) exacerbate this discrepancy. This approximation affects the handling of the free-stream wind conditions regardless of the wake interactions present. Therefore, we expect a consistent bias in the FLOWERS model to underpredict turbine power relative to the Conventional models. The underprediction of power for each turbine in the farm results in a percentage discrepancy in the AEP predictions between the two models that primarily depends on the wind rose and is mostly insensitive to the number of turbines and their layout.

Another significant assumption is that an average wind speed per wind direction is necessary in the FLOWERS model. The Conventional AEP models in this paper also use this assumption, but they have the flexibility to consider a full sweep of wind speeds per wind direction when more accuracy is desired. Higher wind speeds should have a higher weight to their AEP contribution than lower wind speeds because of the nonlinear relationship between wind speed and power. The average wind speed  $\hat{u}_{\infty}$  linearizes the contribution of power from the range of wind speeds, artificially increasing the share of power production from lower-than-average wind speeds and diminishing the share from higher-than-average wind speeds. The overall magnitude and direction of this effect on turbine power prediction depends on the distribution of  $f(u_{\infty}, \phi_{\infty})$  and is difficult to predict a priori. Our analysis of this effect with a Conventional AEP model shows this underprediction to be 5%–10% depending on the wind rose and is independent of the farm layout.

A third assumption is that the power and thrust coefficients are specified as if all turbines are experiencing free-stream velocity ( $C_T(u_{\infty})$  and  $C_P(u_{\infty})$ ) rather than accounting for local flow conditions. We know that in the absence of blockage or terrain effects,  $u_{\infty} \geq u_i$  always.  $C_T(u)$  is a monotonically decreasing function, so  $C_T(u_{\infty}) \leq C_T(u_i)$ . As a result, the wake velocity deficits predicted by FLOWERS are lower in magnitude and the power of downwind turbines would be overpredicted. As for  $C_P$ , in Regions I and II of the power curve, the curve is monotonic nondecreasing, and  $C_P(u_{\infty}) \geq C_P(u_i)$ . FLOWERS would tend to overpredict power in this regime. In Region III,  $C_P$  decreases with wind speed, so  $C_P(u_{\infty}) < C_P(u_i)$ , and FLOWERS would underpredict power. This latter effect would be noticeable when the free-stream wind speed is high ( $u_{\infty}/u_c > 0.5$ ). In practice, we expect these effects to reduce the underprediction of AEP discussed above for wind roses with low to moderate wind speeds.

Lastly, the Fourier representation of the wind rose is approximate with a finite number of Fourier modes. The error of the discrete Fourier transform increases as the number of Fourier modes decreases. Also, it is important to note that the resolution of the wind rose that is input to the Fourier transform determines the maximum number of modes that can be computed ( $M = \text{floor}(D/2) + 1$ ). So FLOWERS is expected to match the Conventional AEP models better when the input wind rose possesses a higher resolution of the wind direction.

### 2.3.2 | AEP Model Inputs

For both the FLOWERS and Conventional models, we assume that the turbine and plant inputs to the AEP models (i.e., turbine positions and power and thrust curves) are known with zero uncertainty. The uncertain model inputs are therefore the wake expansion rate,  $k$ , and the discretized wind condition probability function,  $f(u_{\infty}^{(s)}, \phi_{\infty}^{(d)})$ . The calibration of wake model parameters is notoriously difficult and susceptible to error [42, 43]. We use a standard choice of  $k$  for the Park model of 0.05 for offshore conditions and 0.075 for onshore conditions [44]. However, analysis of wind farm boundary layers suggests

that streamwise turbulence intensity asymptotically increases with downstream rows [45], meaning that a uniform  $k$  neglects the notion of increased turbulence intensity in the downwind regions of wind plants that would encourage the partial recovery of wake losses. Therefore, across the range of expected wind conditions, we might expect FLOWERS to underpredict wind farm power production for larger wind farms compared with smaller wind farms. As for the wind condition variability, assuming sufficiently many samples of the (statistically stationary) atmospheric conditions are available to construct the wind rose, we would expect little uncertainty in the probability estimates of the wind conditions at the site of interest. Lastly, all of these AEP models assume horizontally homogeneous free-stream wind speed, direction, and turbulence intensity in each flow scenario, which are only valid for offshore wind farm flows.

### 3 | Comparative Analysis of AEP Estimates and Cost

#### 3.1 | Randomized Case Study Design

We consider various wind farm cases with randomized model inputs to compare the AEP predictions and cost of AEP evaluations between different models. In this section, we focus on comparisons between FLOWERS and Conventional-Jensen to analyze the modeling differences specific to the FLOWERS derivation (instead of differences between underlying wake models). The Conventional AEP models are implemented in FLORIS [18], an open-source controls-oriented wake modeling software library, and an implementation of the FLOWERS code is available on an open-source repository [46]. The turbines are modeled as NREL 5-MW reference turbines [47], with rotor diameter  $D = 126\text{m}$ .

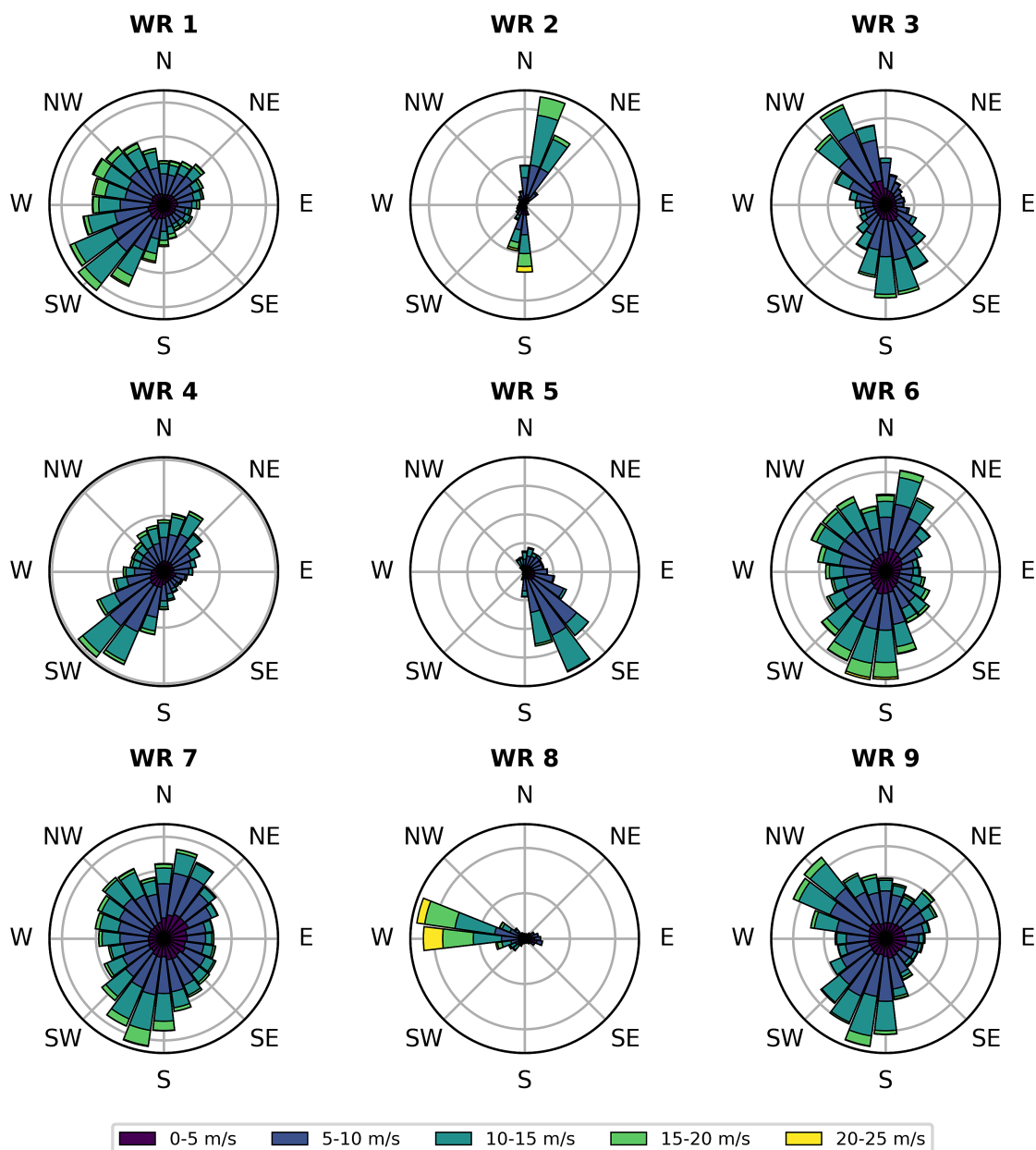


FIGURE 2 | Nine wind roses sampled from the WIND Toolkit [48].

Wind conditions are sampled from the WIND Toolkit [48]. A set of nine roses, as seen in Figure 2, was selected as a sample of directional and speed distributions. These wind roses (referenced as WR  $i$ , where  $i$  is the index in Figure 2) are provided in  $1^\circ$  increments in wind direction. For the Fourier series representation used by FLOWERS, this resolution produces a maximum number of 181 Fourier modes. The wind speed is provided in 1-m/s increments from 1 to 25 m/s, but in our analysis, we use the average wind speed per wind direction for all cases.

To support analysis across a range of wind farm sizes and layouts, we randomly generate cases with different wind farm configurations. First, we randomly select the number of turbines  $N \in [2,500]$ . Then, a random layout is generated by placing the turbines randomly on the nodes of a rectangular array with  $N + 1$  nodes per edge in the  $x$  direction and six nodes per edge in the  $y$  direction, with 3D separation between adjacent nodes. This method of generating wind farm layouts results in a satisfactory range of wind turbine spacing and a constant wind farm power density with respect to the number of turbines without the needless complexity of considering continuous turbine positions.

### 3.2 | Randomized Case Study Results

We first consider 200 randomized cases, with  $D = 72$  wind direction bins for the Conventional model and  $M = 10$  Fourier modes for the FLOWERS model. These choices in resolution

will be addressed throughout Sections 3 and 4. The AEP predictions of the FLOWERS and Conventional-Jensen models are plotted in Figure 3, and the times of the AEP predictions are plotted in Figure 4.

The results in Figure 3 reflect the trends discussed in Section 2.3. First, we observe that FLOWERS underpredicts AEP relative to the Conventional-Jensen model in all cases. The mean, median, and maximum discrepancies are  $-14\%$ ,  $-11\%$ , and  $-33\%$ , respectively. Second, we observe that the magnitude of the AEP discrepancy is strongly correlated with the wind rose and is most pronounced for Wind Roses 2 and 8, which are those with the highest wind speeds (e.g., above 20 m/s). Overall, the FLOWERS method is expected to predict AEP within about 15% of the Conventional-Jensen model, with worse predictive error for strongly directional wind roses or those with high expected wind speeds.

The sensitivity of the FLOWERS AEP predictive error to the wind conditions—rather than particular layouts—does not impact its use for WFLO. Over the course of a WFLO study, the layouts evolve but the wind rose is fixed. The goal of the study is to find a layout that results in the greatest gain in AEP relative to the initial layout; in terms of the abstract “wake avoidance” problem, a layout that produces a relative increase in AEP compared to another layout more successfully avoids wake interactions. The linear correlation of the AEP discrepancies between the models in Figure 3 suggests that the ratio of AEP

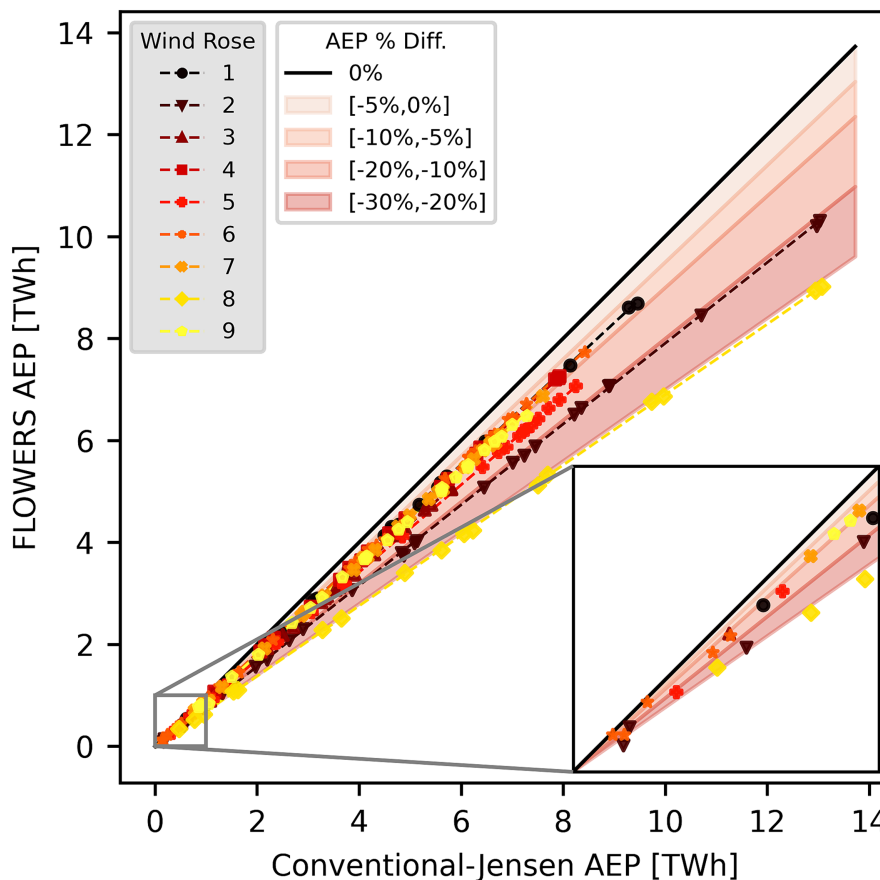


**FIGURE 3** | FLOWERS and Conventional-Jensen AEP predictions for 200 cases with a randomized number of turbines, wind farm layout, and wind rose.

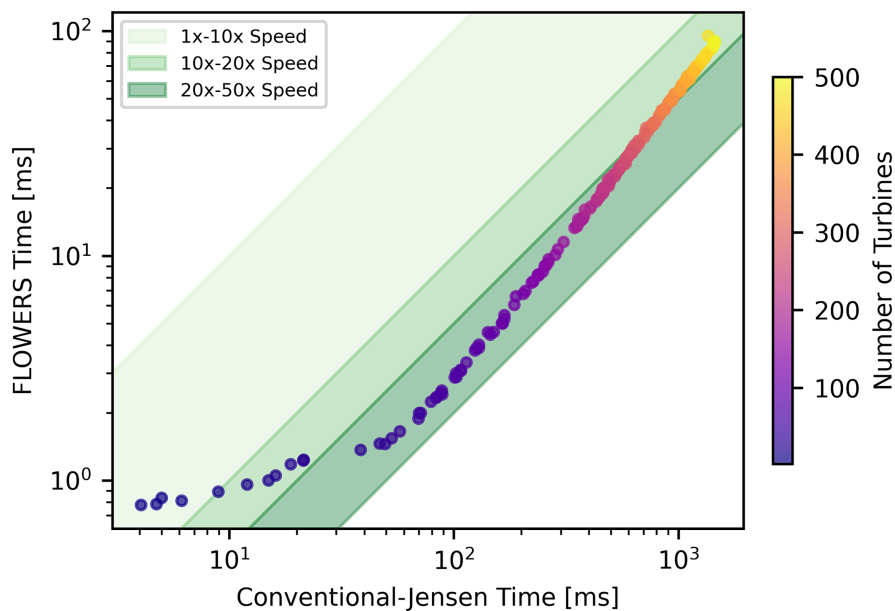


**FIGURE 4** | The cost of FLOWERS and Conventional-Jensen AEP predictions for 200 randomized cases. Computations are performed with a 3.2-GHz Apple M1 CPU.

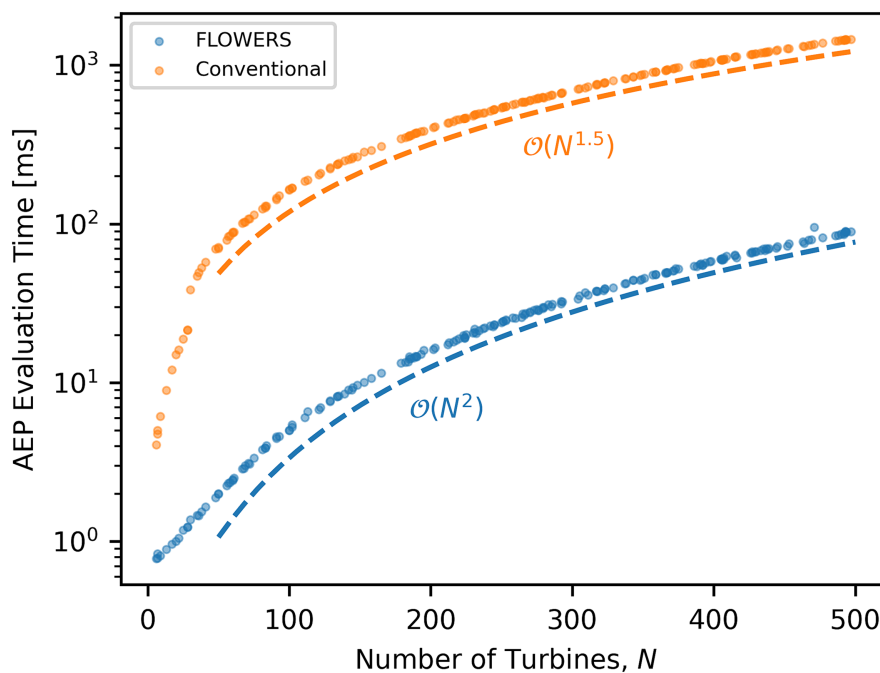


**FIGURE 5** | Cost scaling with wind farm size for the FLOWERS and Conventional-Jensen models across 200 cases. The approximate scaling relationships (dashed lines) were fit to the data (markers).

between two different layouts should be roughly equivalent between the models. Therefore, we expect that FLOWERS is able to quantify the avoidance of wakes in an equivalent way to the Conventional-Jensen model.

Meanwhile, Figure 4 presents a comparison of the cost of the AEP evaluation for each of the 200 layouts with the FLOWERS and Conventional-Jensen approaches. The plot indicates that both models can evaluate AEP for a wind farm with up to 500 turbines in about a second or less, which satisfies the requirement

of a low-cost AEP prediction for WFLO. However, FLOWERS is 10–40 times faster than the Conventional-Jensen model at the specified resolutions, making it a more attractive option.

Figure 4 shows that the cost of the AEP evaluation scales with the number of turbines,  $N$ . Figure 5 plots the evaluation time as a function of the number of turbines for both models to more clearly visualize this trend. As expected from Equation (16), cost scales with  $N^2$  for FLOWERS. Meanwhile, the Conventional model cost scales roughly with  $N^{1.5}$ ; the FLORIS code is

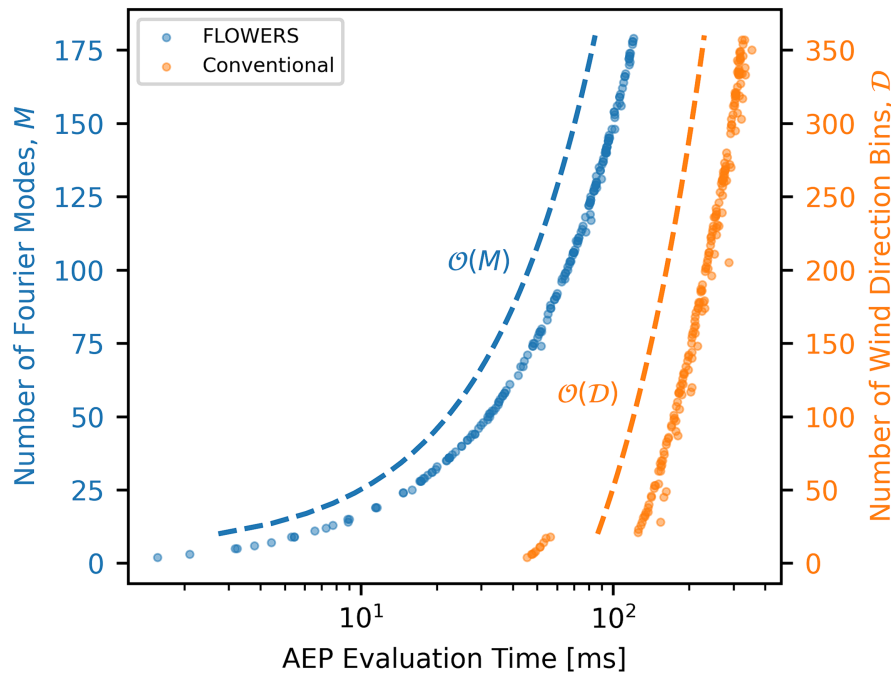


**FIGURE 6** | Cost scaling with model resolution for the FLOWERS and Conventional-Jensen models across 200 cases. The approximate scaling relationships (dashed lines) were fit to the data (markers).

constructed to compute wake interactions in serial order from upstream to downstream turbine, which avoids the quadratic scaling of the FLOWERS model. Even for large wind farms of 500 turbines, FLOWERS is still significantly faster than the Conventional AEP model.

We also expect the cost to scale with the resolution of the models, that is, the number of Fourier terms,  $M$ , for FLOWERS and the number of wind direction bins,  $D$ , for the Conventional AEP model. To analyze this effect, we consider a new set of 200 randomized cases with a fixed number of  $N = 100$  turbines, and we vary  $M$  and  $D$  when performing the AEP evaluations. Figure 6 illustrates the observed trend for AEP evaluation time as a function of  $M$  in the FLOWERS model and  $D$  in the Conventional model. As expected from Equations (28) and (43), cost scales linearly with each of these parameters. As a result, one might suggest reducing the resolution of the models in order to reduce the cost of the AEP prediction and, by extension, the WFLO study. The effect of resolution on the AEP predictions and WFLO design space is explored in the next section.

#### 4 | Objective Function Design Space Analysis

We perform two different analyses aimed at investigating how the choice of the AEP model and its resolution affects the objective function behavior in WFLO problems. First, we consider a wind farm of nine turbines arranged in a three-by-three array with  $7D$  spacing. The wind conditions are defined by WR 7 from Figure 2. We use the three models introduced in Section 2 to estimate the AEP of this wind farm: FLOWERS, Conventional-Jensen, and Conventional-Gauss. We also consider these three models at three different resolutions:  $M = [10, 20, 100]$  for FLOWERS and  $D = [36, 72, 360]$ , corresponding to wind

direction bin widths of  $10^\circ$ ,  $5^\circ$ , and  $1^\circ$ , respectively, for the Conventional models. We randomly perturb the position of each turbine with normally distributed random noise  $\mathcal{N}[0, (D/5)^2]$  for 25 iterations and compute AEP at each iteration. Figure 7 presents the turbine positions at the different iterations and the corresponding AEP predictions normalized by the initial AEP for each model.

Regardless of the number of Fourier modes, the FLOWERS model predicts the same trajectory in AEP across these layouts. This insensitivity to resolution confirms previous findings [20] and permits massive improvements in computational speed with little cost to accuracy. At  $M = 10$ , the FLOWERS model estimates AEP about 20 times faster than the maximum resolution  $M = 181$ .

On the other hand, the Conventional-Jensen and Conventional-Gauss models do show sensitivity to the resolution of the wind direction bins. Between the three resolutions, there is no agreement of the Jensen predictions for the trajectory of AEP across these layouts. In fact, at certain iterations, some resolutions predict an increase in AEP where others predict a decrease. The Jensen model struggles at lower resolutions because the discrete wake model produces a highly discontinuous design space where turbines are frequently jumping between binary states inside or outside of a turbine wake. The Gauss model, which has a continuous wake deficit profile, agrees well between the  $1^\circ$  and  $5^\circ$  resolutions, but at  $10^\circ$ , there is some overestimation of the wake losses, and the trend in AEP change between different configurations is inconsistent with the results for the higher resolutions. This result indicates that the coarser numerical integral introduces discontinuities in the AEP predictions. The disagreements observed across the different resolutions used for the Conventional

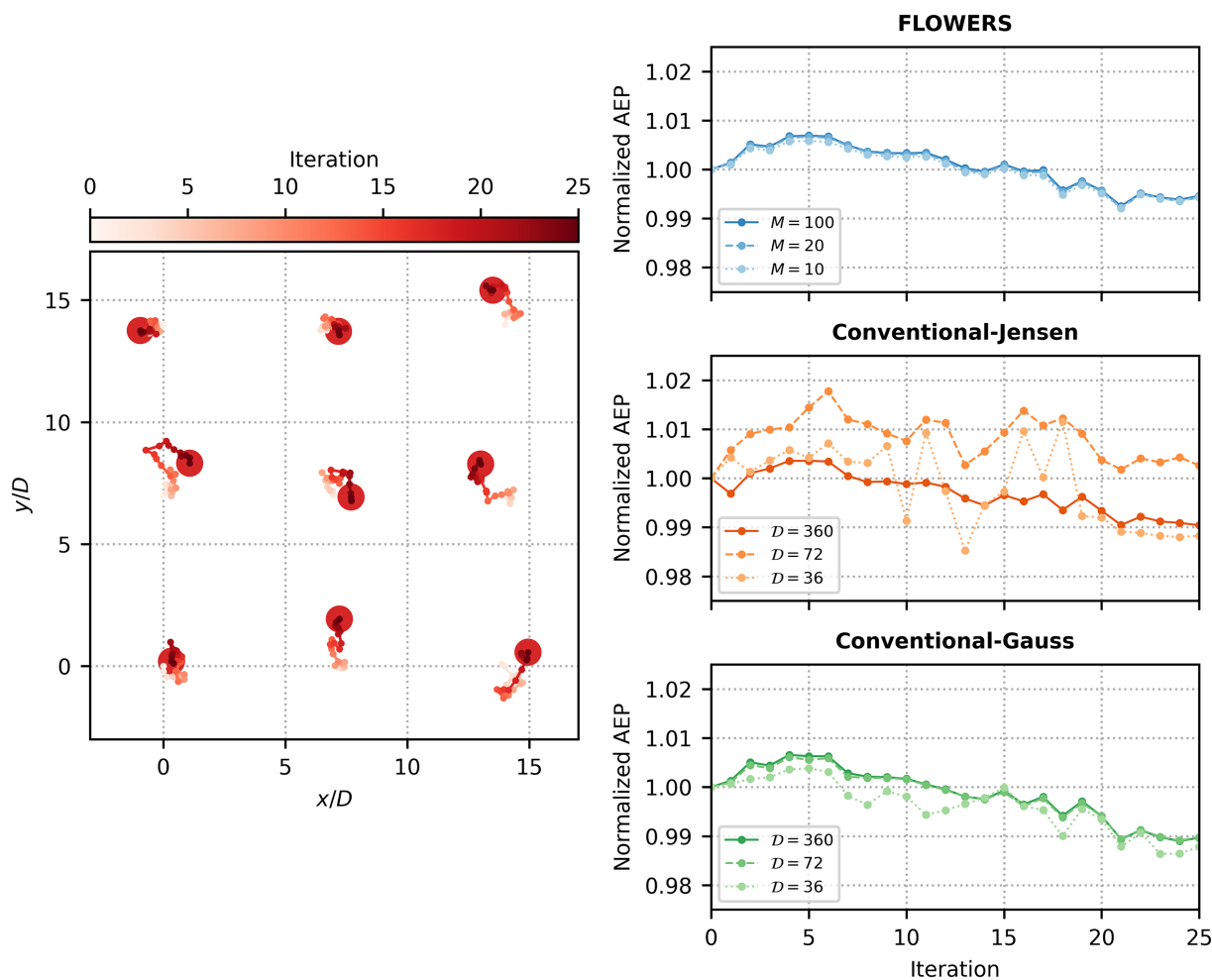


**FIGURE 7** | AEP predictions for a nine-turbine wind farm and WR 7 using the FLOWERS, Conventional-Jensen, and Conventional-Gauss models with random perturbations across 25 iterations. The number of Fourier modes ( $M$ ) for FLOWERS or the number of wind direction bins ( $D$ ) for the Conventional models are varied, with  $D = [360, 72, 36]$  corresponding to wind direction resolutions of  $[1^\circ, 5^\circ, 10^\circ]$ , respectively.

models reveal fundamental differences in their wake avoidance predictions and limit the potential for reducing WFLO cost via reducing the wind direction bin resolution.

Comparison across the models shows that the FLOWERS predictions at all three resolutions, the Conventional-Jensen predictions at  $1^\circ$ , and the Conventional-Gauss predictions at  $1^\circ$  and  $5^\circ$  mostly agree on the trajectory of AEP across the layout iterations. This agreement provides some confidence that the models are predicting the same wake avoidance trends and would perform similarly as the objective function for a WFLO study.

The second analysis aims to further clarify the behavior of the objective function, as provided by the different models at different resolutions, across the design space for a WFLO study. We consider the same wind farm in Figure 7, except we introduce a square boundary for the wind farm and vary the position of the interior turbine in steps of  $0.1D$  while keeping the turbines on the boundaries fixed. We calculate wind farm AEP for all feasible locations for the interior turbine, that is, where the turbine is inside the boundary and separated from all other turbines by at least  $1D$ . This two-dimensional design

space, considering the position of a single turbine, supports conceptualizing and visualizing the behavior of the objective function, and the findings can be expected to extrapolate to the  $2N$  design space of a typical WFLO study. Figure 8 displays contour plots of AEP across the design space of possible interior turbine positions for each AEP model at different choices of resolution. The values are normalized by the maximum AEP across the design space.

The FLOWERS design space is the smoothest in the sense that small changes in turbine position result in similarly small changes in the direction of the AEP gradient. It is visually clear that there are local AEP maxima at the center of the design space and along the top and bottom boundaries; we can postulate that a gradient-based optimization algorithm could traverse this design space easily. We also observe little difference in the design space across different numbers of Fourier modes, which reinforces the trend in Figure 7.

On the other hand, the Conventional-Jensen design space is rife with local optima. It is extremely difficult to visually discern the location of local maxima in AEP, and we could infer that it would be difficult for a gradient-based optimizer to locate

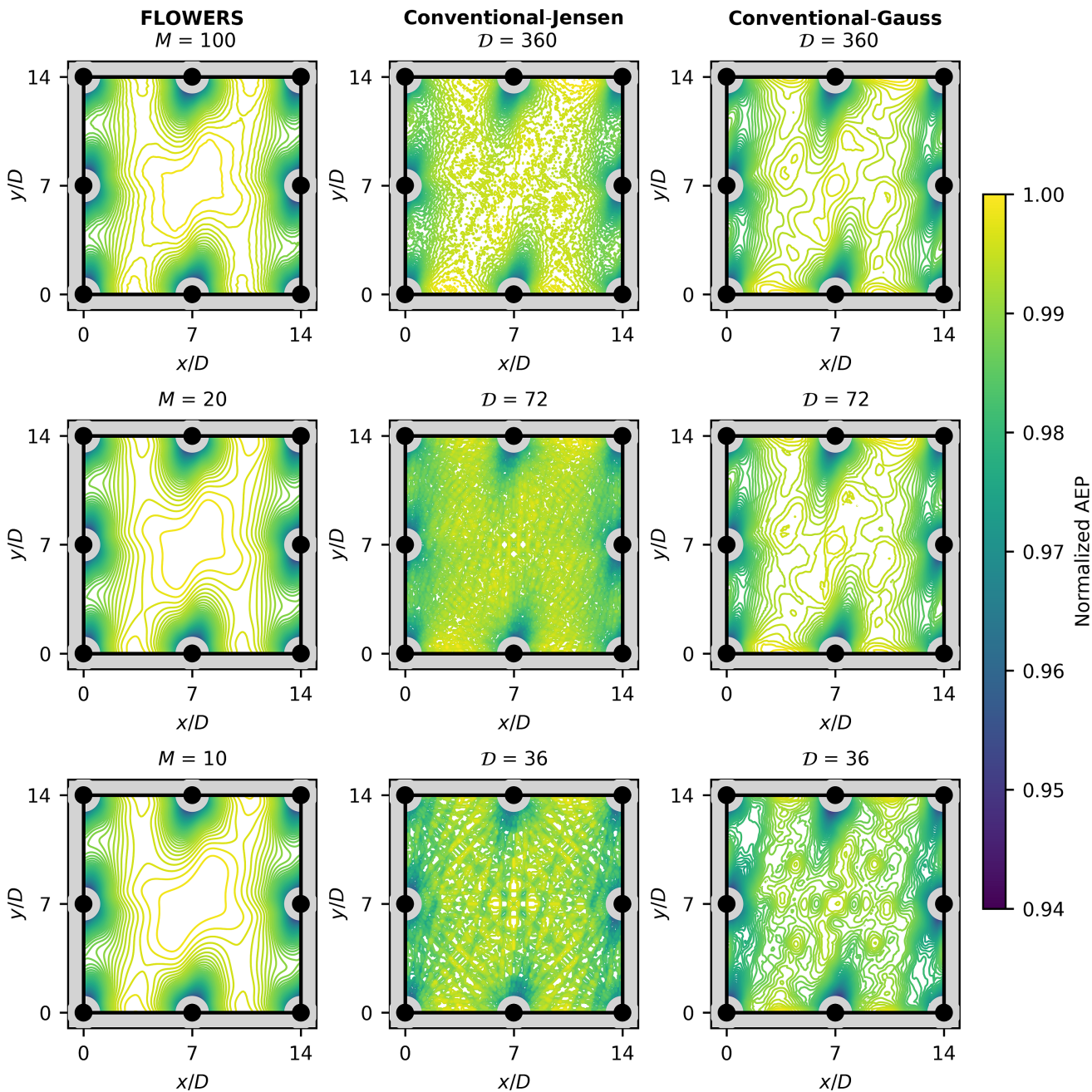


**FIGURE 8** | AEP design space for a single turbine in a wind farm of nine turbines with WR 7 using the FLOWERS (left), Conventional-Jensen (center), and Conventional-Gauss (right). The black circles represent the locations of the eight fixed turbines, and the black lines are the boundary of the wind farm. The number of Fourier modes ( $M$ ) for FLOWERS or the number of wind direction bins ( $D$ ) for the Conventional models decrease from top to bottom. Wind direction bins  $D = [360, 72, 36]$  correspond to wind direction resolutions of  $[1^\circ, 5^\circ, 10^\circ]$ , respectively. Contour lines of normalized AEP are in increments of 0.1%; local gradients are normal to contour lines and local optima are indicated by closed contours.

optimal solutions. Small changes in turbine position yield potentially sharp changes in AEP because of the numerical error of the AEP integral and because of the discrete boundary of the wake. At the highest resolution, the design space is noticeably smoother and begins to resemble the FLOWERS design space.

The Conventional-Gauss design space resides between the FLOWERS and Conventional-Jensen results in terms of qualitative features. At its lowest resolution ( $10^\circ$ ), the design space suffers from the same issues with local optima as the

Conventional-Jensen model; at higher resolutions, the local solutions in the interior of the wind farm are more clear. The smoothness of the continuous Gaussian wake model recovers some of the smoothness in the overall AEP design space, but there is still some coarseness present due to the finite resolution of the numerical integral.

Similar to the discussion around Figure 7, the results in Figure 8 demonstrate that the design spaces for FLOWERS at  $M = 10$ , Conventional-Jensen at  $D = 360$ , and Conventional-Gauss at  $D = 72$  are roughly equivalent. In theory, a

gradient-based algorithm could realistically follow the gradients of these smoother design spaces to arrive at the best local solutions in the center or along the boundaries of the wind farm. Below a certain threshold in the resolution, however, the Conventional AEP models struggle to produce a well-behaved design space for turbine position.

If finite-difference estimates of the AEP gradient are required, it is essential that the objective function is smooth and continuous across the design space. For example, for the Conventional-Jensen model at 5°, finite-difference estimates would likely have significant numerical error that could misinform the optimizer. The analytical functions for the FLOWERS AEP gradient presented in this paper avoid the need for finite-difference estimates, but the smooth behavior of the FLOWERS model across the design space indicates that it should perform better than the Conventional AEP models if finite-difference gradient estimates are required.

## 5 | Layout Optimization Demonstration

We now illustrate the performance of these AEP models in a demonstrative WFLO problem. Consider the following definition:

$$\begin{aligned} & \underset{\mathbf{x}, \mathbf{y}}{\text{minimize}} && -AEP(\mathbf{x}, \mathbf{y}, f), \\ & \text{subject to} && b_i(x_i, y_i, \mathcal{B}) \leq 0 \quad \forall i = \{1, 2, \dots, N\}. \end{aligned} \quad (45)$$

We solve a maximization problem for AEP (expressed as a minimization problem by convention), optimizing over the two independent position coordinates of each turbine. The boundary constraint function for each turbine,  $b_i$ , is defined as the minimum signed distance from the turbine to the boundary polygon defined by the set of points  $\mathcal{B}$  (where a negative distance corresponds to a position within the boundary). A derivation for this boundary function (including analytic derivatives with respect to turbine position) is provided by Criado Risco et al. [25].

We solve this optimization problem with a gradient-based algorithm, specifically the Sparse Nonlinear OPTimizer (SNOPT) [49] implemented with the pyOptSparse wrapper [50]. The optimality and feasibility tolerances are set at  $\epsilon_o = 10^{-3}$  and  $\epsilon_f = 10^{-4}$ , respectively, and the problem functions are scaled such that all of the gradient elements are on the order of 1 or less based on convergence studies. For the FLOWERS objective function, analytical gradients of the objective and constraint functions are provided; for the Conventional objective functions, finite-difference estimates are computed by SNOPT instead.

We compare these three optimizers for the same wind farm discussed in Section 4: a nine-turbine wind farm with a square boundary and expected wind conditions defined by WR 7 (from Figure 2). The initial layout of the wind farm is a three-by-three array with tight 4D spacing. We use the wind condition resolutions discussed in the previous section:  $M = 10$  Fourier modes for FLOWERS,  $D = 72$  wind direction bins for Conventional-Gauss, and  $D = 360$  bins for Conventional-Jensen.

The optimal layouts from each optimizer are seen in Figure 9. The FLOWERS and Conventional-Gauss optimal layouts are almost identical to one another, with slight quantitative differences in turbine positions. This result is consistent with our findings in Section 4 that indicate a similarity between the FLOWERS and Conventional-Gauss design spaces.

We compare the estimated AEP of these different layouts for a more quantitative comparison. We distinguish between the change in the objective function over the course of the optimization study, which we call the objective gain, and the change in the estimated AEP of the initial and optimal layouts in the optimization study, which we call AEP gain. The objective gains in these three studies are as follows: 13.8% for FLOWERS, 10.6% for Conventional-Jensen, and 12.1% for Conventional-Gauss. Due to the modeling differences discussed throughout Sections 2–4, the objective gains can be different even with the same initial and final layouts. So a more fair comparison of the performance of the actual layouts

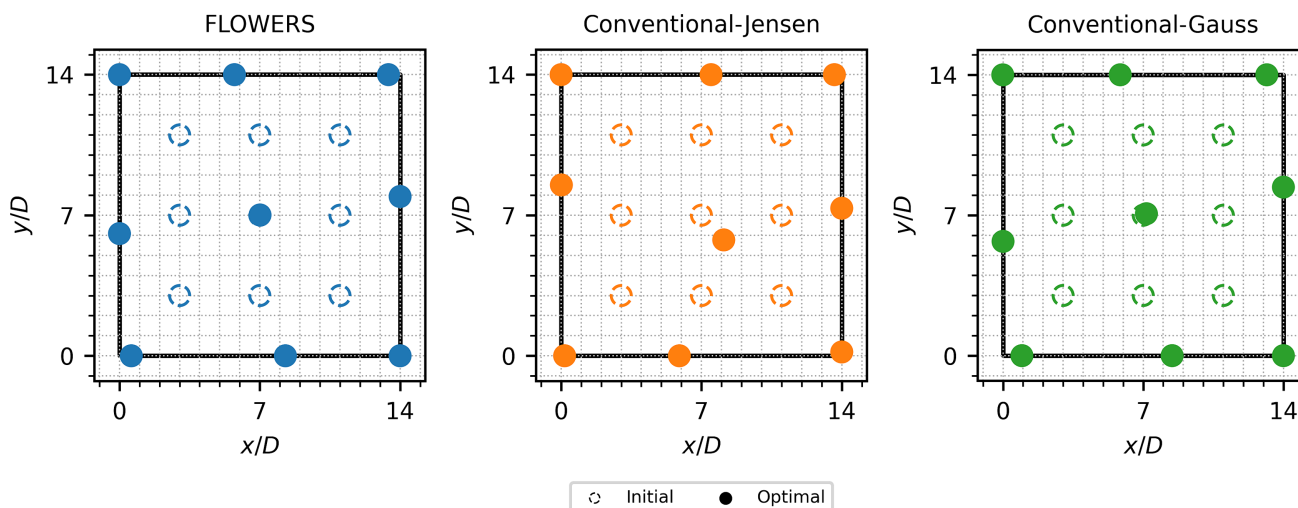


**FIGURE 9** | Initial and optimal layouts from optimization studies using the three different AEP models as an objective function. Solver time in each case is as follows: FLOWERS (1.8s), Conventional-Jensen (58.7s), and Conventional-Gauss (21.5s).

calculates AEP gain with the same AEP model for all three optimal layouts. Using the Conventional-Gauss model, these AEP gains are as follows: 12.1% for FLOWERS, 11.1% for Conventional-Jensen, and 12.1% for Conventional-Gauss. The performance of the FLOWERS and Conventional-Gauss solutions is equal, and both improve over the Conventional-Jensen solution. The FLOWERS and Conventional-Gauss models are better able to navigate toward more optimal solutions compared with the Conventional-Jensen model, which struggles to handle the presumably large number of local optima in the design space. This deficiency with the Conventional-Jensen optimizer was noticeable in previous results [20] and likely worsens as the size of the problem grows.

The major advantage of the FLOWERS model in this example is in computational cost. The wall time required for these studies to converge is as follows: 1.8s for FLOWERS, 58.7s for Conventional-Jensen, and 21.5s for Conventional-Gauss. In other words, the FLOWERS optimizer is able to find roughly the same solution as the Conventional-Gauss optimizer in less than 10% of the time. The additional time for the Conventional-Jensen optimizer is due to the increased wind direction resolution relative to the Conventional-Gauss model. Considering the number of iterations required by the solver, we find that FLOWERS converges after 52 steps, Conventional-Jensen exits after 36 iterations, and Conventional-Gauss exits after 35 iterations. The Conventional-Jensen and Conventional-Gauss optimizers did not converge according to the specified tolerances in SNOPT due to the limited precision of the finite-difference gradient estimates. On the other hand, the FLOWERS optimizer can search for local optima more precisely with its analytical gradient information. Thus, the FLOWERS optimizer is able to pursue the requested convergence accuracy, which explains the higher iteration count in this case. Despite this more exhaustive convergence, the less expensive FLOWERS AEP model and its analytical derivatives composing the AEP gradient are responsible for the overall cost reduction to the WFLO study.

## 6 | Conclusions and Future Work

Our objective in this work was to demonstrate the advantages of using the FLOWERS AEP model over conventional approaches for solving WFLO problems. To the authors' knowledge, FLOWERS is the first analytical, physics-based wake model specifically derived to predict AEP. In this paper, we modified the derivation of the FLOWERS AEP model and expressed it in dimensionless form. We also derived analytical functions for the derivatives of AEP with respect to the position of individual turbines, which are useful alongside a gradient-based optimization algorithm to accelerate the performance of a layout optimization solver.

We then compared the performance of the FLOWERS AEP model with Conventional AEP models (i.e., based on numerical integration across wind conditions) across three metrics. First, we require a low-cost AEP model for WFLO; our results found that FLOWERS is at least an order of magnitude faster than the Conventional alternatives. The FLOWERS AEP predictions were found to be insensitive to the resolution of the model, which enables this significant improvement in cost. Second, we need the

AEP model to reliably quantify the relative difference in wake losses between two layouts. Across a set of randomized layouts, we found agreement in the relative AEP predictions between the FLOWERS model with 10 Fourier modes, the Conventional-Gauss model with 5° wind direction bins, and the Conventional-Jensen model with 1° wind direction bins. Third, we desire the design space of AEP with respect to turbine position to be smooth. We found that the FLOWERS design space was the smoothest between the three models, while the Conventional AEP models required a sufficiently high resolution of the wind direction bins to yield a smooth design space. As a demonstration, we compared the AEP models' performance in a small test layout optimization problem and found that FLOWERS yields a similar optimal layout to the Conventional models in an order of magnitude less time. We acknowledge that these optimization results are limited in their scope and ability to draw general conclusions; in future work, we plan on comparing the performance of FLOWERS and Conventional optimizers more extensively.

Overall, the results presented in this paper demonstrate that the FLOWERS model is well-suited for AEP predictions and layout optimization in homogeneous inflow conditions. The consideration of complex terrain or other effects that produce a heterogeneous flow through the wind farm requires higher-fidelity simulation tools. We also recognize that our study was restricted to the comparison of AEP predictions between various low-fidelity models and we call for further study into cost-effective high-fidelity validation tools for AEP models.

### Acknowledgments

This work was authored in part by the National Renewable Energy Laboratory, operated by Alliance for Sustainable Energy, LLC, for the U.S. Department of Energy (DOE) under Contract No. DE-AC36-08GO28308. Funding is provided by U.S. Department of Energy Office of Energy Efficiency and Renewable Energy Wind Energy Technologies Office. The views expressed in the article do not necessarily represent the views of the DOE or the US government. The US government retains and the publisher, by accepting the article for publication, acknowledges that the US government retains a nonexclusive, paid-up, irrevocable, worldwide license to publish or reproduce the published form of this work, or allow others to do so, for US government purposes.

### Data Availability Statement

The data that support the findings of this study are available from the corresponding author upon reasonable request.

### References

1. J. Herbert-Acero, O. Probst, P.-E. Réthoré, G. Larsen, and K. Castillo-Villar, "A Review of Methodological Approaches for the Design and Optimization of Wind Farms," *Energies* 7, no. 11 (2014): 6930–7016, <http://www.mdpi.com/1996-1073/7/11/6930>.
2. J. Serrano González, M. Burgos Payán, J. M. R. Santos, and F. González-Longatt, "A Review and Recent Developments in the Optimal Wind-Turbine Micro-Siting Problem," *Renewable and Sustainable Energy Reviews* 30 (2014): 133–144, <https://linkinghub.elsevier.com/retrieve/pii/S1364032113006989>.
3. R. Shakoob, M. Y. Hassan, A. Raheem, and Y.-K. Wu, "Wake Effect Modeling: A Review of Wind Farm Layout Optimization Using Jensen's Model," *Renewable and Sustainable Energy Reviews* 58 (2016): 1048–1059, <https://linkinghub.elsevier.com/retrieve/pii/S1364032115016123>.

4. F. Porté-Agel, M. Bastankhah, and S. Shamsoddin, "Wind-Turbine and Wind-Farm Flows: A Review," *Boundary-Layer Meteorology* 174, no. 1 (2020): 1–59, <http://link.springer.com/10.1007/s10546-019-00473-0>.
5. R. J. A. M. Stevens and C. Meneveau, "Flow Structure and Turbulence in Wind Farms," *Annual Review of Fluid Mechanics* 49, no. 1 (2017): 311–339, <https://www.annualreviews.org/doi/10.1146/annurev-fluid-010816-060206>.
6. R. B. Stull, *An Introduction to Boundary Layer Meteorology* (Dordrecht, The Netherlands: Springer, 1988).
7. J. N. Sørensen, "Aerodynamic Aspects of Wind Energy Conversion," *Annual Review of Fluid Mechanics* 43, no. 1 (2011): 427–448, <https://www.annualreviews.org/doi/10.1146/annurev-fluid-122109-160801>.
8. R. J. Barthelmie, S. T. Frandsen, M. N. Nielsen, S. C. Pryor, P. E. Rethore, and H. E. Jørgensen, "Modelling and Measurements of Power Losses and Turbulence Intensity in Wind Turbine Wakes at Middelgrunden Offshore Wind Farm," *Wind Energy* 10, no. 6 (2007): 517–528, <https://onlinelibrary.wiley.com/doi/10.1002/we.238>.
9. R. J. Barthelmie, K. Hansen, S. T. Frandsen, et al., "Modelling and Measuring Flow and Wind Turbine Wakes in Large Wind Farms Offshore," *Wind Energy* 12, no. 5 (2009): 431–444, <https://onlinelibrary.wiley.com/doi/10.1002/we.348>.
10. R. J. Barthelmie, S. C. Pryor, S. T. Frandsen, et al., "Quantifying the Impact of Wind Turbine Wakes on Power Output at Offshore Wind Farms," *Journal of Atmospheric and Oceanic Technology* 27, no. 8 (2010): 1302–1317, <http://journals.ametsoc.org/doi/10.1175/2010JTECHA1398.1>.
11. M. Bastankhah and F. Porté-Agel, "Experimental and Theoretical Study of Wind Turbine Wakes in Yawed Conditions," *Journal of Fluid Mechanics* 806 (2016): 506–541, <https://doi.org/10.1017/jfm.2016.595>.
12. N. O. Jensen, "A Note on Wind Generator Interaction," Risø-M-2411. Risø National Laboratory (Roskilde, Denmark, 1983), OCLC: 1091025164.
13. I. Katic, J. Højstrup, and N. O. Jensen, "A Simple Model for Cluster Efficiency," in *Proceedings of European Wind Energy Conference and Exhibition*, Vol. 1 (Rome: A. Raguzzi, 1986), 407–410.
14. J. P. Murcia, P. E. Réthoré, A. Natarajan, and J. D. Sørensen, "How Many Model Evaluations Are Required to Predict the AEP of a Wind Power Plant?," *Journal of Physics: Conference Series* 625 (2015): 12030, <https://iopscience.iop.org/article/10.1088/1742-6596/625/1/012030>.
15. J. J. Thomas, J. Annoni, P. A. Fleming, and A. Ning, "Comparison of Wind Farm Layout Optimization Results Using a Simple Wake Model and Gradient-Based Optimization to Large Eddy Simulations," in *AIAA Scitech 2019 Forum*, (San Diego, California: American Institute of Aeronautics and Astronautics, 2019), 538, <https://arc.aiaa.org/doi/10.2514/6.2019-0538>.
16. A. Peña, K. Schaldemose Hansen, S. Ott, and M. P. van der Laan, "On Wake Modeling, Wind-Farm Gradients, and AEP Predictions at the Anholt Wind Farm," *Wind Energy Science* 3, no. 1 (2018): 191–202, <https://wes.copernicus.org/articles/3/191/2018/>.
17. J. Schmidt, C.-Y. Chang, M. Dørenkämper, M. Salimi, T. Teichmann, and B. Stoevesandt, "The Consideration of Atmospheric Stability Within Wind Farm AEP Calculations," *Journal of Physics: Conference Series* 749 (2016): 12002, <https://iopscience.iop.org/article/10.1088/1742-6596/749/1/012002>.
18. NREL, *FLORIS* (Golden, Colorado: GitHub, 2023), <https://github.com/NREL/floris>.
19. M. M. Pedersen, A. M. Forsting, P. van der Laan, et al., *PyWake: An Open-Source Wind Farm Simulation tool* (Roskilde, Denmark: DTU Wind, Technical University of Denmark, 2023), <https://gitlab.windenergy.dtu.dk/TOPFARM/PyWake>.
20. M. J. LoCascio, C. J. Bay, M. Bastankhah, G. E. Barter, P. A. Fleming, and L. A. Martínez-Tossas, "FLOW Estimation and Rose Superposition (FLOWERS): An Integral Approach to Engineering Wake Models," *Wind Energy Science* 7, no. 3 (2022): 1137–1151, <https://wes.copernicus.org/articles/7/1137/2022/>.
21. R. Valotta Rodrigues, M. M. Pedersen, J. P. Schøler, J. Quick, and P.-E. Réthoré, "Speeding Up Large-Wind-Farm Layout Optimization Using Gradients, Parallelization, and a Heuristic Algorithm for the Initial Layout," *Wind Energy Science* 9, no. 2 (2024): 321–341, <https://wes.copernicus.org/articles/9/321/2024/>.
22. C. Meneveau, "Big Wind Power: Seven Questions for Turbulence Research," *Journal of Turbulence* 20, no. 1 (2019): 2–20, <https://www.tandfonline.com/doi/full/10.1080/14685248.2019.1584664>.
23. M. P. van der Laan, S. J. Andersen, P.-E. Réthoré, M. Baungaard, J. N. Sørensen, and N. Troldborg, "Faster Wind Farm AEP Calculations With CFD Using a Generalized Wind Turbine Model," *Journal of Physics: Conference Series* 2265, no. 2 (2022): 22030, <https://iopscience.iop.org/article/10.1088/1742-6596/2265/2/022030>.
24. N. F. Baker, A. P. Stanley, J. J. Thomas, A. Ning, and K. Dykes, "Best Practices for Wake Model and Optimization Algorithm Selection in Wind Farm Layout Optimization," in *AIAA Scitech 2019 Forum*, (San Diego, California: American Institute of Aeronautics and Astronautics, 2019), 1–18, <https://arc.aiaa.org/doi/10.2514/6.2019-0540>.
25. J. Criado Risco, R. Valotta Rodrigues, M. Friis-Møller, J. Quick, M. Mølgaard Pedersen, and P.-E. Réthoré, "Gradient-Based Wind Farm Layout Optimization With Inclusion and Exclusion Zones," *Wind Energy Science* 9, no. 3 (2024): 585–600, <https://wes.copernicus.org/articles/9/585/2024/wes-9-585-2024.pdf>.
26. P. A. Fleming, A. Ning, P. M. O. Gebraad, and K. Dykes, "Wind Plant System Engineering Through Optimization of Layout and Yaw Control," *Wind Energy* 19, no. 2 (2016): 329–344, <https://onlinelibrary.wiley.com/doi/10.1002/we.1836>.
27. P. Gebraad, J. J. Thomas, A. Ning, P. Fleming, and K. Dykes, "Maximization of the Annual Energy Production of Wind Power Plants by Optimization of Layout and Yaw-Based Wake Control," *Wind Energy* 20, no. 1 (2017): 97–107, <https://onlinelibrary.wiley.com/doi/10.1002/we.1993>.
28. A. S. Padrón, J. Thomas, A. P. J. Stanley, J. J. Alonso, and A. Ning, "Polynomial Chaos to Efficiently Compute the Annual Energy Production in Wind Farm Layout Optimization," *Wind Energy Science* 4, no. 2 (2019): 211–231, <https://wes.copernicus.org/articles/4/211/2019/>.
29. J. Quick, P.-E. Rethore, M. Mølgaard Pedersen, R. V. Rodrigues, and M. Friis-Møller, "Stochastic Gradient Descent for Wind Farm Optimization," *Wind Energy Science* 8, no. 8 (2023): 1235–1250, <https://wes.copernicus.org/articles/8/1235/2023/>.
30. A. P. J. Stanley, J. King, and A. Ning, "Wind Farm Layout Optimization With Loads Considerations," *Journal of Physics: Conference Series* 1452, no. 1 (2020): 12072, <https://iopscience.iop.org/article/10.1088/1742-6596/1452/1/012072>.
31. A. P. J. Stanley and A. Ning, "Massive Simplification of the Wind Farm Layout Optimization Problem," *Wind Energy Science* 4, no. 4 (2019): 663–676, <https://wes.copernicus.org/articles/4/663/2019/>.
32. J. J. Thomas, N. F. Baker, P. Malisani, et al., "A Comparison of Eight Optimization Methods Applied to a Wind Farm Layout Optimization Problem," *Wind Energy Science* 8, no. 5 (2023): 865–891, <https://wes.copernicus.org/articles/8/865/2023/>.
33. R. King, A. Glaws, G. Geraci, and M. S. Eldred, "A Probabilistic Approach to Estimating Wind Farm Annual Energy Production With Bayesian Quadrature," in *AIAA Scitech 2020 Forum*, (Orlando, FL: American Institute of Aeronautics and Astronautics, 2020), 1951, <https://arc.aiaa.org/doi/10.2514/6.2020-1951>.
34. J. J. Thomas and A. Ning, "A Method for Reducing Multi-Modality in the Wind Farm Layout Optimization Problem," *Journal of Physics: Conference Series* 1037 (2018): 42012, <https://iopscience.iop.org/article/10.1088/1742-6596/1037/4/042012>.

35. D. Guirguis, D. A. Romero, and C. H. Amon, "Gradient-Based Multi-disciplinary Design of Wind Farms With Continuous-Variable Formulations," *Applied Energy* 197 (2017): 279–291, <https://linkinghub.elsevier.com/retrieve/pii/S0306261917304269>.
36. D. Guirguis, D. A. Romero, and C. H. Amon, "Toward Efficient Optimization of Wind Farm Layouts: Utilizing Exact Gradient Information," *Applied Energy* 179 (2016): 110–123, <https://linkinghub.elsevier.com/retrieve/pii/S0306261916308765>.
37. M. J. Kochenderfer and T. A. Wheeler, *Algorithms for Optimization* (Cambridge, Massachusetts: MIT Press, 2019).
38. J. J. Thomas, P. M. O. Gebraad, and A. Ning, "Improving the FLOWRIS Wind Plant Model for Compatibility With Gradient-Based Optimization," *Wind Engineering* 41, no. 5 (2017): 313–329, <http://journals.sagepub.com/doi/10.1177/0309524X17722000>.
39. P. B. S. Lissaman, "Energy Effectiveness of Arbitrary Arrays of Wind Turbines," *Journal of Energy* 3, no. 6 (1979): 323–328, <https://arc.aiaa.org/doi/10.2514/3.62441>.
40. A. Niayifar and F. Porté-Agel, "Analytical Modeling of Wind Farms: A New Approach for Power Prediction," *Energies* 9, no. 9 (2016): 741, <http://www.mdpi.com/1996-1073/9/9/741>.
41. A. Crespo and J. Hernández, "Turbulence Characteristics in Wind-Turbine Wakes," *Journal of Wind Engineering and Industrial Aerodynamics* 61, no. 1 (1996): 71–85, <https://linkinghub.elsevier.com/retrieve/pii/016761059500033X>.
42. M. F. Howland, A. S. Ghate, and S. K. Lele, "Influence of the Geostrophic Wind Direction on the Atmospheric Boundary Layer Flow," *Journal of Fluid Mechanics* 883 (2020): A39, [https://www.cambridge.org/core/product/identifier/S0022112019008899/type/journal\\_article](https://www.cambridge.org/core/product/identifier/S0022112019008899/type/journal_article).
43. J. Schreiber, C. L. Bottasso, B. Salbert, and F. Campagnolo, "Improving Wind Farm Flow Models by Learning From Operational Data," *Wind Energy Science* 5, no. 2 (2020): 647–673, <https://wes.copernicus.org/articles/5/647/2020/>.
44. R. J. Barthelmie, G. C. Larsen, S. T. Frandsen, et al., "Comparison of Wake Model Simulations With Offshore Wind Turbine Wake Profiles Measured by Sodar," *Journal of Atmospheric and Oceanic Technology* 23, no. 7 (2006): 888–901, <http://journals.ametsoc.org/doi/10.1175/JTECH1886.1>.
45. M. Calaf, C. Meneveau, and J. Meyers, "Large Eddy Simulation Study of Fully Developed Wind-Turbine Array Boundary Layers," *Physics of Fluids* 22, no. 1 (2010): 15110, <http://aip.scitation.org/doi/10.1063/1.3291077>.
46. M. J. LoCascio, *FLOWERS* (Stanford, California: GitHub, 2024), <https://github.com/locascio-m/flowers>.
47. J. Jonkman, S. Butterfield, W. Musial, and G. Scott, "Definition of a 5-MW Reference Wind Turbine for Offshore System Development," NREL/TP-500-38060. (Golden, Colorado: National Renewable Energy Laboratory, 2009), <http://www.osti.gov/servlets/purl/947422-nhrlni/>.
48. C. Draxl, A. Clifton, B.-M. Hodge, and J. McCaa, "The Wind Integration National Dataset (WIND) Toolkit," *Applied Energy* 151 (2015): 355–366, <https://linkinghub.elsevier.com/retrieve/pii/S0306261915004237>.
49. P. E. Gill, W. Murray, and M. A. Saunders, "SNOPT: An SQP Algorithm for Large-Scale Constrained Optimization," *SIAM Review* 47, no. 1 (2005): 99–131, <http://epubs.siam.org/doi/10.1137/S0036144504446096>.
50. N. Wu, G. Kenway, C. Mader, J. Jasa, and J. Martins, "pyOptSparse: A Python Framework for Large-Scale Constrained Nonlinear Optimization of Sparse Systems," *Journal of Open Source Software* 5, no. 54 (2020): 2564, <https://joss.theoj.org/papers/10.21105/joss.02564>.